and tensin homolog induced kinase-1 (PINK1) (Valente et al., 2004), and leucine-rich repeat kinase-2 (LRRK2) (Paisan-Ruiz et al., 2004; Zimprich et al., 2004). α-Synuclein, UCH-L1 and LRRK2 are linked to the autosomal dominant form of PD, whereas parkin, DJ-1 and PINK1 are linked to the recessive form.

In 1998, UCH-L1 carrying an Ile to Met mutation at amino acid position 93 (I93M) was identified in one German family affected by autosomal dominant familial PD. UCH-L1, also known as PGP9.5, is an abundant protein in neuronal cells, comprising up to about 1–2% of total protein in the brain. Its function as de-ubiquitylating enzyme (Larsen et al., 1998; Wilkinson et al., 1989), ubiquitylating enzyme (Liu et al., 2002), de-neddylating enzyme (Hemelaar et al., 2004), and mono-ubiquitin stabilizer (Osaka et al., 2003) has been reported. In vitro analysis using recombinant human UCH-L1 indicated that I93M mutation results in the reduction of hydrolase activity of about 50% (Nishikawa et al., 2003). Uchl1 gene deletion in mice, however, was reported to causes gracile axonal dystrophy (gad), a recessive neurodegenerative disease with distinct phenotype and pathological features from PD (Saigoh et al., 1999). Moreover, extensive analysis failed to find other PD patients with mutations in the UCHL1 gene (Lincoln et al., 1999; Maraganore et al., 1999) and there was an incomplete penetrance in reported German family (Leroy et al., 1998). Thus, the correlation of I93M mutation and pathogenesis of PD was questioned.

To elucidate the pathological role of UCH-L1^{I93M} expression in the pathogenesis of PD, in vivo, we generated transgenic mice expressing human UCH-L1^{I93M}.

2. Experimental procedures

2.1. Generation of hUCHL1^{WT} and hUCHL1^{I93M} transgenic mice

We generated transgenes by cloning either the wild-type or I93M mutant human UCH-L1 cDNAs under the control of the human platelet-derived growth factor B chain (PDGF-B) promoter (Fig. 1A) (Sasahara et al., 1991). Sequences encoding UCHL1 were amplified from a human brain cDNA library (Stratagene, La Jolla, CA) by PCR and subcloned into the XhoI and NotI sites of pCI-neo (Promega, Madison, WI). The I93M substitution was obtained using QuikChange (Stratagene). The 5′ flanking region of the human PDGF-B chain gene was isolated from the human genomic DNA and inserted into the BglII and XhoI site of pCI-neo which results in the replacement of promoter from CMV to PDGF-B. The plasmid was linearized by digestion with HindIII and AatII. A 2 μg/ml solution of the linearized plasmid of each transgene was then micro-injected into the pronuclei of newly fertilized C57BL/6J mouse eggs. Offspring were screened for the presence of the transgene by PCR of tail DNA using specific primers (forward: PD-UCH-2, 5′-GCACTCTCCCTTCTCCTTTATA-3′; reverse: PD-UCH-5, 5′-CCTGTATGGCCTCATTCTTTTC-3′). Expression of hUCH-L1^{I93M} in a low-expressing mouse line only occurred in male mice. Thus, all experiments were done using male heterozygous transgenic mice. Animal care and handling were in accordance with institutional regulations for animal care and were approved by the Animal Investigation Committee of the National Institute of Neuroscience, National Center of Neurology and Psychiatry, Tokyo, Japan which conforms the National Institute of Health guide for the care and use of Laboratory animals.

2.2. Quantitative RT-PCR analysis

Primers specific for mouse Uchl1 (forward: mL1-7, 5′-CCTTGGTTTGCAG-CTTTAGCA-3′; reverse: mL1-8, 5′-GGGCTGTAGAACGCAAGAAGA-3′)
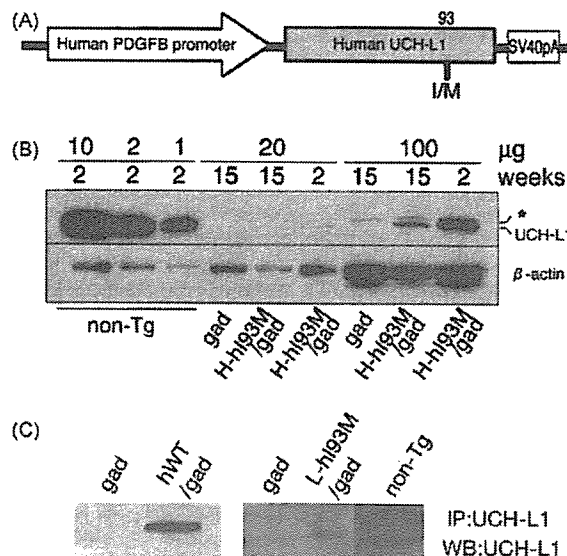

Fig. 1. Generation of transgenic mice expressing hUCH-L1^{WT} and hUCH-L1^{I93M}. (A) UCH-L1^{I93M} was constructed under control of the PDGF-B promoter, as depicted. (B) Immunoblotting analysis of endogenous mouse UCH-L1 and transgenic human UCH-L1 expression in mouse midbrain. To detect exogenous human UCH-L1 levels specifically, we generated transgenic mice in the gad background (H-hI93M/gad), which corresponds to the null mutant of Uchl1. Notice that the faint band corresponding to UCH-L1 is detected at 2 weeks of age when 20 μg protein/lane was loaded for the detergent-soluble fraction of midbrain origin in H-hI93M/gad mice. When the applied protein was increased to 100 μg/lane, UCH-L1 was easily detected at 2 weeks in H-hI93M/gad mice, and UCH-L1 levels markedly decreased by age 15 weeks. Faint bands indicated by the asterisk may correspond to UCH-L3, which cross-reacted with the UCH-L1 antibody when a large amount of protein was loaded per lane. (C) Immunoprecipitation analysis of exogenous human UCH-L1 in hWT/gad (left) and L-hI93M/gad (right) brains. Brain lysates from hWT/gad (left) or L-hI93M/gad (right) were both immunoprecipitated and detected using anti-UCH-L1 antibody. The band corresponding to the UCH-L1 can be found in both hWT/gad and L-hI93M/gad lysates but not in gad lysates indicating the exogenous human UCH-L1 expression.

and human UCHL1 (forward: L1Tg-F2, 5′-TGGCAACTTCTCCTCCTGCA-3′; reverse: L1Tg-R2, 5′-ACAGCACTTTGTTCAGCATC-3′) were designed, and SYBR Green-based real-time quantitative RT-PCR was performed using the ABI PRISM 7700 (Applied Biosystems, Foster City, CA) using total RNA from mouse brain (n = 3 for each line) (Aoki et al., 2002). GAPDH was used as an internal control.

2.3. Fractionation and immunoblotting and immunoprecipitation

For the immunoblotting of total UCH-L1, the soluble fraction in RIPA (20 mM Tris–HCl, pH 7.5; 0.1% SDS; 1.0% (w/v) Triton X-100; 1.0% sodium deoxycholate) with Complete EDTA-Free Protease Inhibitors (Roche, Basel, Switzerland) was extracted from H-hI93M/gad ([high-expressing] UCH-L1$^{I93M/-}$, Uchl1$^{gad/gad}$), gad and non-Tg mouse midbrains. The extracted samples were loaded as indicated in Fig. 1.

For subfractionation, the cortex and hippocampus were removed from the midbrains of a H-hI93M mouse or a non-Tg littermate and bottom half under the aqueduct were used as the substantia nigra fraction. The fractionation method was modified from that of Kahle et al. (2001). Each sample was homogenized with 9 volumes of 5% SDS/TBS lysis buffer (50 mM Tris–HCl (pH 7.5), 150 mM NaCl, 5% SDS) with Complete EDTA-Free Protease Inhibitors using a 23G syringe. After three times of 10 s sonication, samples were ultra-centrifuged in 130.000 × g for 1 h, and the supernatant were pooled as 5% SDS fraction. The pellets were washed with 5% SDS/TBS solution once and further homogenized in 8 M urea/5% SDS/TBS lysis buffer

(8 M urea, 5% SDS, 50 mM Tris–HCl (pH 7.5), 150 mM NaCl) with 23G syringe. The resulting supernatant was used as 8 M urea/5% SDS fraction. The protein concentration was assessed by a DC-protein assay kit (Bio-Rad). 1.25 µg of 5% SDS fraction and 0.5 µg of 8 M urea/5% SDS fraction were subjected to SDS-PAGE using 15% gels (Perfect NT Gel; DRC, Tokyo, Japan). Anti-UCH-L1 (1:5000, RA95101; Ultraclone, Isle of Wight, UK) and anti-β-actin (1:5000, clone AC15; Sigma, St. Louis, MO) were used to detect each protein. Signals were detected using a chemiluminescent SuperSignal West Dura Extended Duration Substrate kit or West Femto Maximum Sensitivity Substrate kit (Pierce, Rochford, IL) and analyzed with a ChemiImager (Alpha Innotech, San Leandro, CA). For the internal control of 8 M urea/5% SDS fraction, 1 µg protein were dot blotted to PVDF membrane and stained with Ponceau S staining (Rane et al., 2004). Statistical analyses were conducted using the two-tailed Student's *t*-test with total of four samples for each group.

For the immunoprecipitation, half of the brain (for hWT/gad) or midbrain region (for L-hI93M/gad) were homogenized in 2 ml ice-cold modified RIPA buffer (50 mM Tris–HCl, pH 7.4; 1% (w/v) Nonidet P40; 0.25% sodium deoxycholate; 150 mM NaCl; 1 mM EDTA) with Complete EDTA-Free Protease Inhibitors and centrifuged at 16,000 × g at 4 °C for 20 min. The protein concentration of the resulting supernatants was determined with the Protein Assay Kit (Bio-Rad, Hercules, CA). Immunoprecipitation was performed with a Seize X Mammalian Immunoprecipitation kit (Pierce, Rockford, IL) with some modifications. Briefly, 300 µg of protein was added to a 50 µl slurry of immobilized protein G cross-linked with rabbit polyclonal anti-human UCH-L1 (AB1716; Chemicon, Temecula, CA) or normal rabbit IgG and rotated at 4 °C overnight. The samples were then washed three times with 500 µl of 0.1B buffer (20 mM Tris–HCl, pH 8.0; 0.1 M KCl; 5 mM MgCl₂; 10% (w/v) glycerol; 0.1% (w/v) Tween 20; 10 mM β-mercaptoethanol). Elution of samples was performed by adding 20 µl of 5× SDS-PAGE sample buffer, and samples were boiled at 100 °C for 5 min.

2.4. Immunohistochemistry, immunofluorescence and electron microscopy

Brain and peripheral (sciatic) nerve sections from 2-, 7- and 20-week-old mice were analyzed (n = 3 for each line) by immunocytochemistry as previously described (Wang et al., 2004; Watanabe et al., 1977) using antibodies to UCH-L1 (1:4000; RA95101, Ultraclone), TH (1:1000; Chemicon) and ubiquitin (1:1000; Sigma–Aldrich, St. Louis, MO). Antibody binding was detected with 3,3′-diaminobenzidine tetrachloride (DAB) or 3-amino-9-ethylcarbazole (AEC) as a peroxidase substrate or Alexa-488- or Alexa-568-conjugated secondary antibodies (Invitrogen, Carlsbad, CA). Sections were then counterstained with hematoxylin. Ultrastructural electron microscopic studies of the substantia nigra were performed as described (Watanabe et al., 1977) using midbrain sections.

2.5. MPTP treatment

For MPTP treatment, the mice received four injections of 30 mg/kg MPTP–HCl intraperitoneally (Research Biochemicals, Natick, MA) in saline at 24-h intervals (Mochizuki et al., 2001).

2.6. Tyrosine hydroxylase-positive cell counting and biochemical analysis

Samples for both histochemistry and biochemical analysis were obtained from the same mouse. Each animal was deeply anesthetized with pentobarbital and perfused transcardially with 10 ml of ice-cold phosphate-buffered saline, and the brain was removed and divided into forebrain and midbrain–hindbrain regions.

For the tyrosine hydroxylase (TH)-positive cell counting, midbrain–hindbrain was fixed with chilled 4% formaldehyde solution (pH 7.4). The procedure of TH-positive cell counting was described previously (Furuya et al., 2004) with minor modifications. Briefly, the substantia nigra was cut into serial sections (30 µm), and every third section was subjected to

immunostaining for TH using a polyclonal antibody to TH (a kind gift from I. Nagatsu, Fujita Health University, Aichi, Japan). The Vectorstain Elite ABC kit (Vector Labs, Burlingame, CA) was used for subsequent antibody detection with DAB as a peroxidase substrate. The number of viable TH-positive neurons was assessed by manual counting by a blind observer using coded slides (Furuya et al., 2004). The number of total neuronal cells outside the substantia nigra was counted after Bodian staining in the cerebral cortex (1 mm², seven regions per section), cerebellum (total of all lobules) and hippocampus (total number in CA1, CA2, CA3 and dentate gyrus). Statistical analysis were done by one-way ANOVA followed by post hoc test (Fisher's PLSD).

For the biochemical analysis, the striatum was quickly dissected from the forebrain, and the striatal tissue samples were weighed (~30 mg) and homogenized in 10 volumes (w/v) of ice-cold 0.05 M sodium acetate (pH 6.0). Homogenates were centrifuged (18,000 × g, 10 min at 4 °C), and the supernatant was frozen immediately on dry ice and stored frozen at −80 °C until use.

For the striatal dopamine measurement, supernatant (50 µl) from the striatal lysate was mixed with an equal volume of 0.2 M perchloric acid containing 0.2 mM EDTA and centrifuged (18,000 × g, 10 min at 4 °C), and the supernatant was applied to an HPLC system. Chromatographic separation was achieved using a C18 reversed-phase column (150 mm × 4.6 mm i.d., Model S-100; TOSOH, Tokyo, Japan). The mobile phase (50 mM citrate, 50 mM NaH₂PO₄, 0.1 mM EDTA, 4.36 mM 1-heptanesulfonate, 2.35% acetonitrile, 5.72% MeOH, pH 2.5) was pumped through the chromatographic system at a rate of 1.0 ml/min. A Coulochem electrode array system (ESA Inc., MA) with eight coulometric electrodes was used to quantify the eluted catecholamines and their metabolites. Statistical analysis was done by one-way ANOVA followed by post hoc test (Fisher's PLSD).

TH activity was assayed following the method of Hooper (1997) with minor modifications (Hooper et al., 1997; Naoi et al., 1988). The incubation mixture contained 50 µl of diluted sample and included the following components in a total volume of 200 µl: 0.2 M sodium acetate (pH 6.0), 0.2 M glycerol, 20,000 U/ml catalase, 1.0 mM 6-MPH4, 4.0 U/ml dihydropteridine reductase, 1 mM NADPH and 200 µM L-tyrosine. Incubations were carried out at 37 °C for 10 min in a shaking water bath. Reactions were terminated by adding 600 µl of ice-cold 0.33 M perchloric acid, 17 mM EDTA including 50 pmol of α-methyl DOPA as the internal standard. The L-DOPA produced was extracted onto alumina, and the catechols were eluted with 0.16 M acetic acid followed by 0.02 M phosphoric acid. A sample incubated on ice instead of 37 °C was used as a blank. The amount of L-DOPA was quantified with the HPLC system, as mentioned above. Statistical analysis was done by one-way ANOVA.

2.7. Silver staining

Sixty-micrometer brain sections from 12-week-old mice (n = 3 for each group) were stained using FD NeuroSilver kit (FD Neuro-Technologies, Catonsville, MD) according to the manufacturer's protocol to detect argyrophilic grain-positive degenerating neurons.

2.8. Behavioral tests

H-hI93M mice and non-Tg littermates were used for all behavioral analyses. For the accelerated rota-rod test, 20–25-week-old mice were placed on the rod (Ohara, Japan) at a speed of 5 rpm, and the speed was accelerated to 50 rpm in 5 min. The length of time that each mouse was able to remain on the rod before falling was recorded. For the locomotor activity test, 11–13-week-old or 20–23-week-old mice were placed separately in a home cage 4 days before the beginning of analysis for habituation. Two to four mice were monitored at once for locomotor activity on the home cage monitor (Ohara, Japan) for 63 h beginning from 5:30 p.m. All mice were housed with a 12 h light/dark cycle, with the light cycle beginning at 8 a.m. The last 12 h of active night were used for the analysis. Mice were weighed after the analysis; there were no differences between the weights H-hI93M and non-Tg mice (data not shown). Statistical analyses were conducted using the two-tailed Student's *t*-test.

3. Results

3.1. Generation of transgenic mice expressing human UCHL1[193M] in neurons of the substantia nigra

The human *PDGF-B* promoter was used to drive expression of the human *UCHL1* in Tg mice (Fig. 1A) (Sasahara et al., 1991). Germline transmission of *hUCHL1*[193M] was obtained in two independent Tg mouse lines (denoted L-hI93M and H-hI93M, where L and H denote low and high expression, respectively). Germline transmission of *hUCHL1*[WT] was obtained in one Tg mouse line (denoted hWT). The levels of transgenic mRNA and endogenous *Uchl1* mRNA were assessed by quantitative RT-PCR using primers designed to amplify specifically the *UCHL1* transgene and mouse *Uchl1*, respec-

tively. The estimated relative expression of *UCHL1* among the transgenic lines was H-hI93M > hWT > L-hI93M. The ratio of endogenous mouse *Uchl1* transcripts to transgenic human *UCHL1* transcripts was 111 in H-hI93M, 739 in hWT and 6015 in L-hI93M ($n = 3$ for each line).

At the amino acid level, human and mouse UCH-L1 differ at only 11 discrete positions, and endogenous UCH-L1 is one of the most abundant protein in the brain. Therefore, we were not able to make distinction between the exogenous human UCH-L1 and endogenous mouse UCH-L1 in the brains of Tg mice (data not shown) using immunoblotting analysis with several antibodies against human UCH-L1 from different companies (Chemicon; UltraClone; Medac; Biogenesis). To ascertain the expression of transgene product, we used *gad* mice, which lack endogenous UCH-L1 (Saigoh et al., 1999). We mated mice
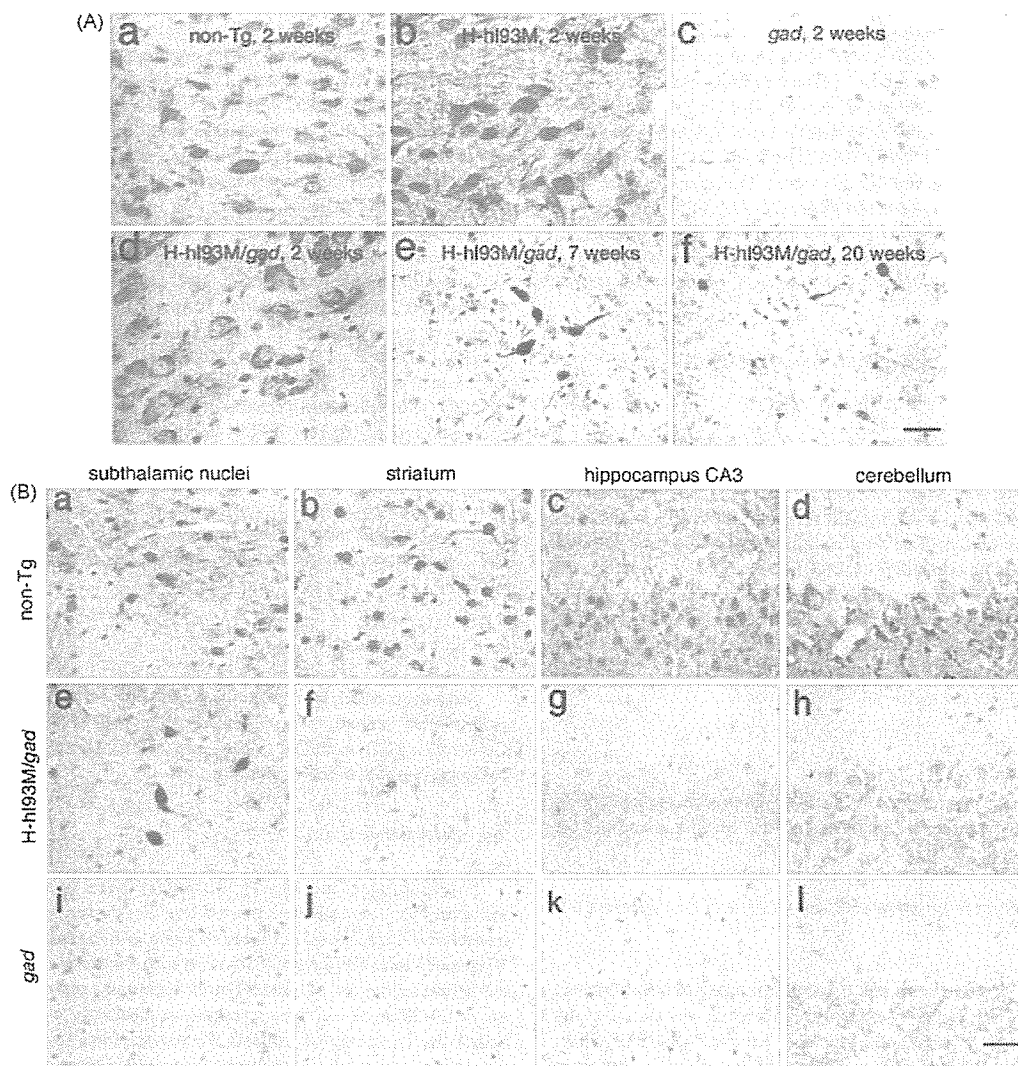

Fig. 2. Immunohistochemistry of UCH-L1 in coronal sections of the substantia nigra (A) and regions outside the substantia nigra (B) in H-hI93M, H-hI93M/*gad* and non-Tg mice. (A) Non-Tg mice (a), H-hI93M mice on a C57BL/6J background (b) and *gad* mice (c) at 2 weeks of age and H-hI93M/*gad* mice at 2 weeks (d), 7 weeks (e) and 20 weeks (f) of age. Neurons expressing UCH-L1 in the substantia nigra decreased in number and area, and densely stained neurons were observed in the aged substantia nigra. Scale bar: 30 μm. (B) UCH-L1 immunohistochemistry of coronal sections at the level of the subthalamic nuclei (a, e, i), striatum (b, f, j), hippocampus CA3 (c, g, k) and cerebellum (d, h, l). Upper row (a–d), non-Tg mice; middle row (e–h), H-hI93M/*gad* mice; lower row (i–l), *gad* mice. All mice were examined at 2 weeks of age. Scale bar: 30 μm.

from each transgenic line with mice homozygous for the $Uchl1^{gad/gad}$ allele (*gad* mice). Detergent-soluble (1% Triton X-100) fractions of mouse midbrain from H-hI93M/*gad* ($UCHL1^{I93M/-}$, $Uchl1^{gad/gad}$) at 2 and 15 weeks of age were subjected to SDS-PAGE and immunoblotted with anti-UCH-L1. We detected human UCH-L1 expression in H-hI93M/*gad* brains (Fig. 1B). Compared with endogenous mouse UCH-L1, which constitutes 1–2% of neuronal proteins, human UCH-L1 expression was substantially lower in H-hI93M/*gad* brains (~1% of endogenous UCH-L1 at 2 weeks of age; Fig. 1B). Interestingly, the level of transgenic human UCH-L1 was lower at 15 weeks than at 2 weeks of age (Fig. 1B). Although we could not detect human UCH-L1 in L-hI93M/*gad* and hWT/*gad* by standard immunoblotting methods, we were successful in detecting it by immunoprecipitation (Fig. 1C). These data suggest the expression of the human UCH-L1 in L-hI93M and hWT mice, which were much lower than in H-hI93M mice.

UCH-L1 is a cytosolic protein predominantly expressed in neuronal cells including dopaminergic neurons at substantia nigra with diffuse localization (data not shown). Thus, we next examined the immunohistochemical localization of the transgene products. In agreement with the data obtained by

Western blotting analysis, UCH-L1-immunoreactive cells were not observed in any brain region, including the substantia nigra, of the L-hI93M/*gad* and hWT/*gad* mice (data not shown). In H-hI93M/*gad* mice, however, human UCH-L1^{I93M} was detected in the substantia nigra, the region that contains the central pathological lesions in PD, with relatively high intensities (Fig. 2A). Subthalamic nuclei, striatum, hippocampus CA3 and cerebellum also contained UCH-L1 immunoreactive cells in H-hI93M/*gad* mice (Fig. 2B). As with the previous report that CAT expression under control of the *PDGF-B* promoter in transgenic mice localizes to neuronal cell bodies (Sasahara et al., 1991), most UCH-L1-immunoreactive cells in H-hI93M/*gad* mice had a neuronal morphology (Fig. 2). Western blotting analysis of midbrain lysates showed a reduction of transgenic UCH-L1^{I93M} at 15 weeks of age as compared with that at 2 weeks in H-hI93M/*gad* mice (Fig. 1B). Thus, we also performed immunohistochemical analysis of UCH-L1 on substantia nigra from 2-, 7- and 20-week-old H-hI93M/*gad* mice. We found many UCH-L1-positive neurons at 2 weeks. The number of positive cells had decreased by 7 weeks, however, at which time small-sized and densely stained neurons were observed, and UCH-L1-positive cells were barely
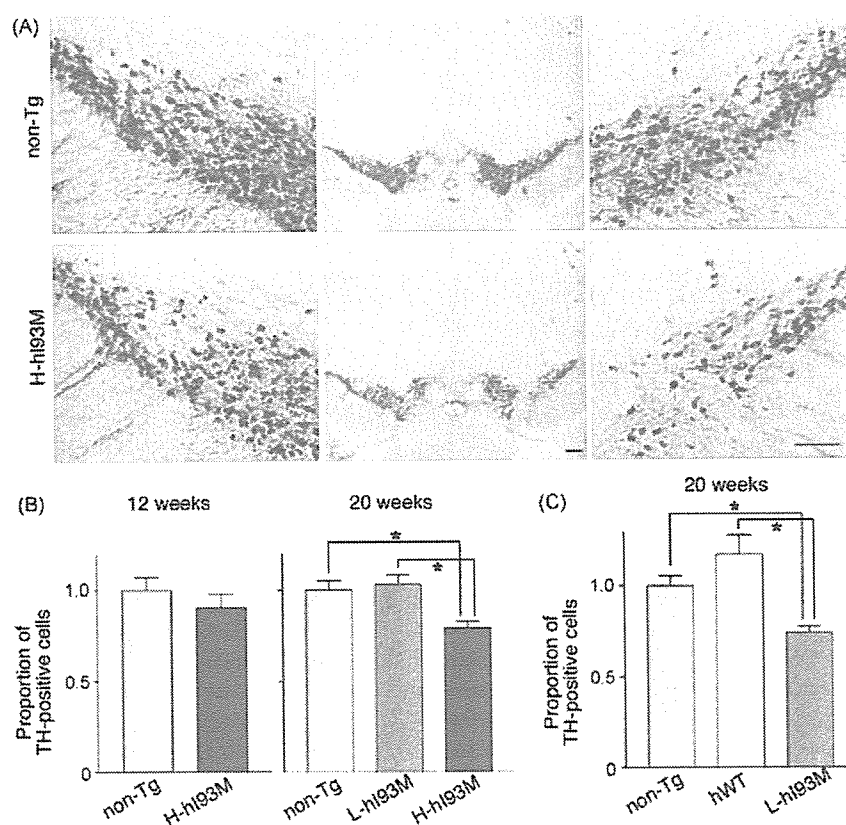

Fig. 3. TH-positive neurons of hI93M Tg mice were reduced as the animals aged. (A) Immunohistochemical staining of the substantia nigra with anti-TH in non-Tg (upper panels) and H-hI93M (lower panels) mice at 20 weeks of age. Scale bar: 1 mm. Left and right panels in the figure correspond to the left and right part of the middle panel, respectively. (B) Proportion of neurons stained with anti-TH in the substantia nigra from non-Tg and hI93M mice at 12 weeks (left panel) and 20 weeks (right panel) of age. Cell numbers were normalized to those for the non-Tg mice. Values are the mean ± S.E.M.; $n = 10$ Significance was examined by a one-way ANOVA. $^*p < 0.01$. (C) The number of TH-positive cells in the substantia nigra from 20-week-old non-Tg ($n = 5$), hWT ($n = 3$) and L-hI93M mice ($n = 5$) after treatment with MPTP. The cell numbers were normalized to those for non-Tg mice. Values are the mean ± S.E.M. Significance was examined by a one-way ANOVA. $^*p < 0.001$.

detectable at 20 weeks of age (Fig. 2A). Together, our results indicate that hUCH-L1^{I93M} is expressed in the neurons of the substantia nigra in H-hI93M mice, but the number of positive cells declines before 20 weeks of age. With the failure to detect hUCH-L1 protein in hWT/*gad* mice and L-hI93M/*gad* mice both in the Western blotting and the immunohistochemistry, we performed most of the analysis using H-hI93M mice with non-Tg mice as a control.

3.2. Loss of dopaminergic neurons in the substantia nigra of 20-week-old H-hI93M mice

We next determined whether the number of midbrain dopaminergic neurons was reduced in the substantia nigra of transgenic mice using TH immunohistochemistry. The number of TH-positive dopaminergic neurons in the substantia nigra at the same neuroanatomical level was compared and quantified for each transgenic mouse line. Surprisingly, we detected an

~30% reduction in TH-positive neurons in 20-week-old H-hI93M mice as compared with those in non-Tg control mice (Fig. 3A and B). This reduction was not seen in 12-week-old H-hI93M mice or 20-week-old L-hI93M mice. Together with the decrease in the level of UCH-L1^{I93M} (Fig. 1B) and the reduction in UCH-L1-positive neurons in the substantia nigra of H-hI93M/*gad* mice, our data indicate that UCH-L1^{I93M} expression in the dopaminergic neurons is sufficient to induce the degeneration of these neurons.

MPTP is a toxin used to induce an acute Parkinsonian syndrome that is indistinguishable from sporadic PD (Dauer and Przedborski, 2003). MPTP metabolite 1-methyl-4-pyridinium (MPP$^+$), an inhibitor of complex I of the mitochondrial respiration chain, is taken up by the terminals of dopaminergic neurons via the dopamine transporter (DAT), thereby causing the selective death of nigral neurons (Dauer and Przedborski, 2003). Although neuronal loss was not observed in L-hI93M mice at 20 weeks of age, we speculated that dopaminergic
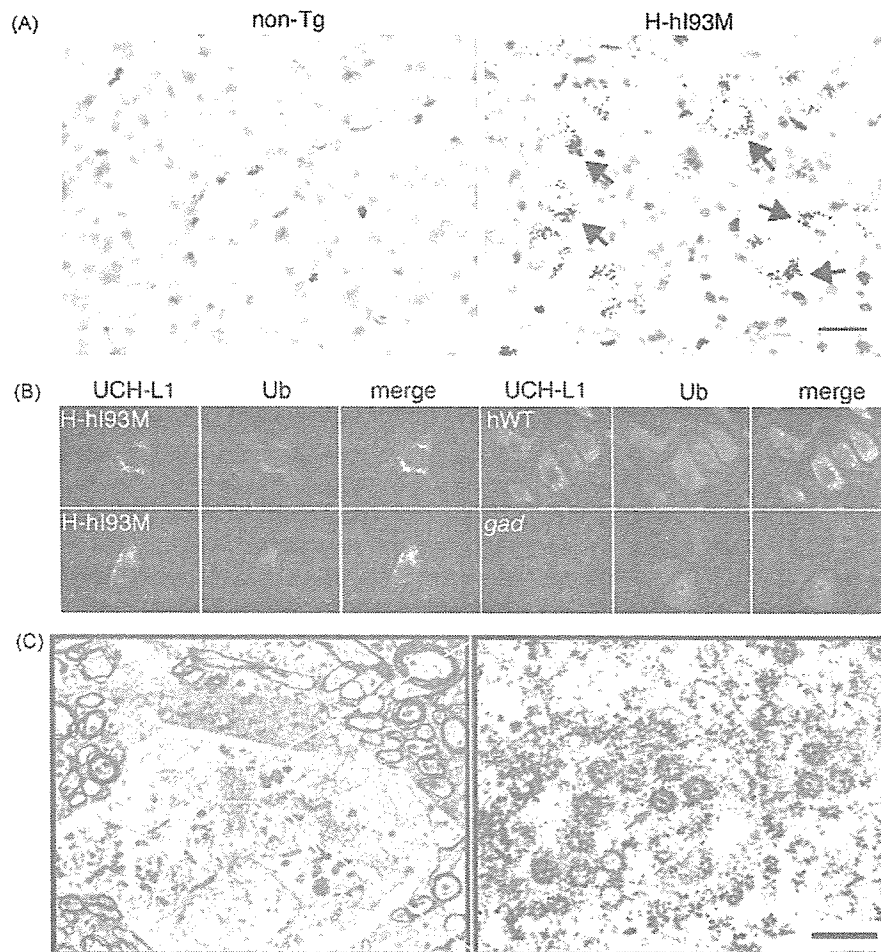

Fig. 4. Several neuropathological features reminiscent of PD are present in H-hI93M mice brains. (A) Silver staining of the substantia nigra at 12 weeks of age in non-Tg and H-hI93M mice. Note the presence of silver staining-positive argyrophilic grains in the cell bodies of some dopaminergic neurons in H-hI93M mice (arrows). This kind of abnormal structure was not seen in substantia nigra of non-Tg mice. Scale bar: 30 μm. (B) Confocal images of dopaminergic neurons from hWT, H-hI93M and *gad* mice. H-hI93M mice showed the formation of ubiquitin-positive cytoplasmic inclusions (red) co-localized with UCH-L1 staining (green) in the remaining nigral neurons at 20 weeks of age. Compared with the diffuse, reduced staining of ubiquitin in *gad* mice, nigral neurons from hWT mice also showed a diffuse pattern of staining but with fine small granular cytoplasmic staining (red) co-localized with UCH-L1 (green). (C) Electron micrographs of a nigral neuron from a 20-week-old H-hI93M mouse at the level of the cell body (left panel), and dense-core vesicles (red arrows) at higher magnification (right panel). Scale bar: 1 μm.

neurons of L-hI93M mice might be more susceptible to MPTP toxin compared to that of non-Tg mice or hWT mice. As expected, significantly fewer TH-positive neurons were observed in L-hI93M mice after MPTP treatment as compared with hWT or non-Tg control mice though hWT express higher *hUCHL1* compared to L-hI93M (Fig. 3C). The number of TH-positive neurons in MPTP-treated hWT mice was somewhat higher than that in non-Tg mice ($p < 0.001$). Taken together with the fact that expression of human UCH-L1 in L-hI93M is lower than that in hWT, these results suggest that the UCH-L1^{I93M} mutant, but not UCH-L1^{WT}, is specifically toxic to dopaminergic neurons.

3.3. Presence of neuropathology in dopaminergic neurons from H-hI93M mice

To evaluate the degenerative process of dopaminergic neurons, silver staining was used to indicate argyrophilic degenerating neurons (Lo Bianco et al., 2004). In non-Tg mice, no silver staining was observed, whereas scattered neurons containing grains that were silver staining positive were present in the substantia nigra of H-hI93M mice (Fig. 4A). The presence of intracellular inclusions called Lewy bodies and Lewy neurites are neuropathological characteristics of PD and are silver staining positive (Sandmann-Keil et al., 1999; Uchihara et al., 2005). It is also known that UCH-L1 and ubiquitin, as well as α-synuclein, are components of Lewy bodies (Lowe et al., 1990). Furthermore, UCH-L1 is tightly associated with mono-ubiquitin *in vivo* (Osaka et al., 2003). Thus, we expected that the silver staining-positive grains might have characteristic features of Lewy bodies. We therefore compared the immunohistochemical analysis of UCH-L1 and ubiquitin. Compared with reduced staining for ubiquitin in *gad* mice, strong and diffuse ubiquitin staining was observed in nigral neurons of hWT mice and non-Tg mice (data not shown), and this staining co-localized with UCH-L1, which is in agreement with our previous report (Osaka et al., 2003). In H-hI93M substantia nigra at 20 weeks of age, ubiquitin- and UCH-L1-positive cytoplasmic inclusions, a large aggregates with different morphology from small dots usually seen in hWT mice and non-Tg mice, were observed in a portion of the remaining nigral neurons (Fig. 4B). These inclusions were, however, α-synuclein or hematoxylin–eosin (HE) negative (data not shown). We could not observe UCH-L1- and ubiquitin-positive inclusions in L-hI93M mice (data not shown).

Another cellular characteristic of PD neuropathology is dense-core vesicles of about 80–200 nm in perikarya, which are frequently observed along with Lewy bodies in PD patients (Watanabe et al., 1977). We observed electron dense-core vesicles in the cytoplasm of ~30% of nigral neurons in H-hI93M mice using electron microscopy (Fig. 4C). In non-Tg mice, such vesicles with a similar shape were not detected in cell bodies but rather were seen in synaptic terminals. Taken together, our data indicate that degenerating dopaminergic neurons in the substantia nigra of H-hI93M mice are devoid of Lewy bodies but show some neuropathological features such as silver staining-positive argyrophilic grains, aggregates with UCH-L1 and ubiquitin, and dense-core vesicles in the perikarya.

3.4. Increased amount of SDS-insoluble but urea/SDS-soluble UCH-L1 in the midbrain of H-hI93M mice

UCH-L1^{I93M} has reduced α-helical content as compared with UCH-L1^{WT} (Nishikawa et al., 2003), and UCH-L1^{I93M} overexpression in COS7 cells results in more cells that contain cytoplasmic inclusions (Ardley et al., 2004). Thus, the presence of UCH-L1-positive inclusions in H-hI93M dopaminergic neurons led us to speculate whether UCH-L1^{I93M} would be less soluble than the wild-type protein *in vivo*. To biochemically characterize the changes in UCH-L1 deposited in the brains of H-hI93M mice, we sequentially extracted frozen midbrain tissues with 5% SDS (soluble fraction) and 8 M urea/5% SDS (insoluble fraction) and analyzed each fraction by immuno-blotting with anti-UCH-L1. As expected, immunoblots of insoluble fractions showed a modest but statistically significant increase in UCH-L1 in the midbrains of H-hI93M mice as compared with those from a non-Tg mouse (Fig. 5A and B), indicating increased insolubility of UCH-L1^{I93M} *in vivo*, which might have resulted in dopaminergic neurotoxicity.

3.5. Decreased dopamine content in the striata of H-hI93M mice

Because the nigro-striatal pathway is severely affected in PD patients, and because our mice showed the degeneration of dopaminergic neurons in the substantia nigra, we evaluated the nerve terminals in the striatal pathway using
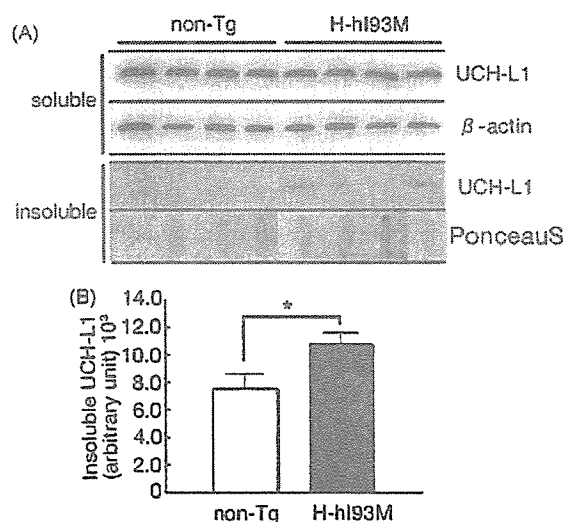

Fig. 5. Protein insolubility of UCH-L1 in H-hI93M Tg mice. (A) Immunoblotting analysis of UCH-L1 in soluble (5% SDS soluble) and insoluble (5% SDS insoluble and 8 M urea/5% SDS soluble) fractions from tissue containing the substantia nigra (11–13 weeks). Soluble fraction (5 μg for each) was probed with anti-UCH-L1 or anti-β-actin. Insoluble fraction (0.5 μg for each) was probed with anti-UCH-L1. One microgram of each insoluble fraction was applied to dot blotting and stained by Ponceau S to show that each fraction contained the same amount of total protein. A slight increase in the insolubility of UCH-L1 in the substantia nigra fraction from H-hI93M mice is seen as compared with that from non-Tg mice. (B) The experiment was done with H-hI93M mice and non-Tg littermates from five different litters, and the results of quantitative analyses in insoluble fraction is shown ($n = 5$ mice for each group).
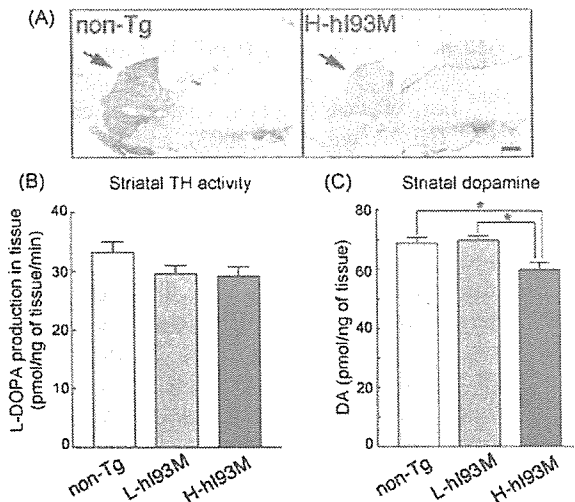
Fig. 6. H-hI93M mice show pathology in the striatum. Dopamine content and TH activity were lower in H-hI93M mice. (A) Sagittal sections from non-Tg and H-hI93M mice at 20 weeks of age were immunostained with the dopaminergic marker anti-TH. TH immunoreactivity is decreased in the nigro-striatal axons (arrows) of H-hI93M brains. Scale bar: 100 μm. (B) TH activity and (C) dopamine content were measured following extraction and homogenization of the mouse striatum of non-Tg, L-hI93M and H-hI93M mice at 20 weeks of age ($n = 4$; mean ± S.E). Significance was examined by a one-way ANOVA. *$p < 0.05$.
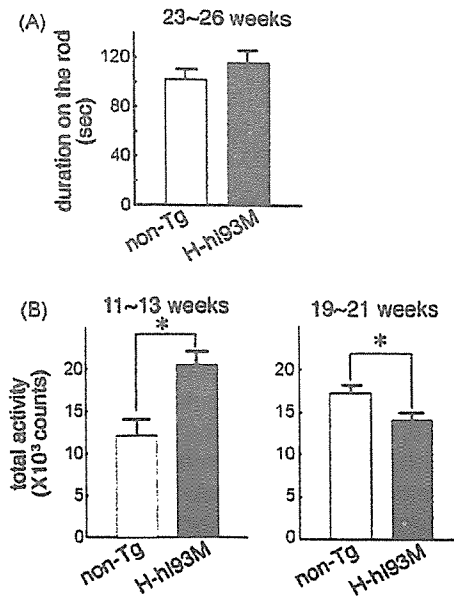
Fig. 7. H-hI93M transgenic mice show locomotor deficits. (A) Accelerated rota-rod analysis of H-hI93M and non-Tg mice ($n = 6$ for non-Tg and $n = 7$ for H-hI93M) at 23–26 weeks of age. Mice were placed on a rod, and their duration on the rod before falling off (mean value of three trials for each animal) was recorded. (B) Home cage monitor analysis of H-hI93M and non-Tg mice at 11–13 weeks of age (left; $n = 4$ for each line) and at 19–21 weeks of age (right; $n = 8$ for non-Tg and $n = 10$ for H-hI93M). Note the significant hypolocomotion of H-hI93M mice as compared with non-Tg mice at 19–21 weeks of age. Values are the mean ± S.E.M. Significance was examined using the unpaired Student's t-test. *$p < 0.05$.

immunohistochemical and biochemical analyses. In agreement with the reduction of TH-positive dopaminergic neurons in the substantia nigra, nigro-striatal fibers in H-hI93M mice showed decreased immunoreactivity for TH as compared with that of non-Tg mice (Fig. 6A). TH activity, analyzed by determining L-DOPA production in the striatal tissues, also showed a tendency to decline in H-hI93M mice, although it was not significantly different (Fig. 6B). Loss of dopaminergic neurons in the substantia nigra and decreased TH activity in the striatum of H-hI93M mice prompted us to examine the concentration of striatal dopamine. Compared with non-Tg mice, H-hI93M mice showed a significant reduction of dopamine content in the striatum (Fig. 6C).

3.6. Decreased spontaneous, voluntary movements of H-hI93M mice

Given the prominent loss of dopaminergic neurons in the substantia nigra and the reduction in dopamine content in the striatum of H-hI93M mice, we next assessed the locomotor abilities of H-hI93M mice using a battery of well-established behavioral tests. Involuntary movement was analyzed by the rota-rod test (Goldberg et al., 2005) on 23–26-week-old mice. H-hI93M mice and non-Tg mice were similarly able to maintain their balance on the rotating rod during rod acceleration before falling off (Fig. 7A). We next analyzed spontaneous, voluntary movements with a locomotor activity test (Goldberg et al., 2005). Unexpectedly, 11–13-week-old H-hI93M mice showed significant hyperlocomotion during active periods (i.e., at night) as compared with non-Tg mice during home cage monitoring (Fig. 7B). However, 19–21-week-old H-

hI93M mice showed a modest but significant reduction in locomotor activity during active periods as compared with non-Tg mice (Fig. 7B). These results indicate that, in addition to the neuropathological changes, H-hI93M mice exhibit mild behavioral deficits related to PD.

4. Discussion

In this study, we characterized transgenic mice expressing hUCH-L1^{I93M}, a mutation with presumptive association with familial PD, in the brain. Our previous attempt of making mouse UCH-L1^{WT} Tg mice under various higher expressing promoters, such as EF1α, resulted in an infertility of mice, thus it was impossible to maintain the lines. This failure resulted from the effect of overexpressing UCH-L1 in the testis/ovary leading to an increased apoptosis in these reproductive organs, although we did not find obvious morphological differences in the brain (Wang et al., 2006). Thus, we used PDGF-B promoter in this study to avoid massive expression of the transgene.

Two lines of hUCH-L1^{I93M} Tg mice and one line of hUCH-L1^{WT} Tg mice were viable and fertile without any predictable abnormalities. All of the three Tg lines expressed very limited levels of the human UCHL1 gene with a maximum transcript ratio of about 1/100 as compared with the endogenous mouse Uchl1. However, immunohistological analysis indicated that higher level of hUCH-L1^{I93M} expression could be detected in the large number of neurons in the substantia nigra of

H-hI93M/gad mice at 2 weeks of age. In addition, there is a difference in the morphology of hUCH-L1^{I93M} expressing neurons, reminiscent of dying neurons, in the substantia nigra of H-hI93M/gad mice among 7 and 20 weeks of age. We also observed an eventual decline in the number of UCH-L1-positive neurons in H-hI93M/gad mice, as they age. Furthermore, the dopaminergic neurons in the substantia nigra of H-hI93M mice at 12 weeks of age showed silver staining-positive argylophilic grains, which represent neurons undergoing degeneration (Lo Bianco et al., 2004). Since we observed a loss of dopaminergic neurons in the substantia nigra and reduced dopamine content in the striatum of H-hI93M mice at 20 weeks of age, our results indicate the possibility that hUCH-L1^{I93M} expressing dopaminergic neurons degenerate with age.

In addition to cell loss, several neuropathological features were observed in the substantia nigra of H-hI93M mice. Dopaminergic neurons had (1) electron dense-core vesicles in the perikarya, and (2) cytoplasmic inclusions that were positive for both UCH-L1 and ubiquitin. Despite these features, we did not observe eosinophilic or α-synuclein-positive Lewy bodies at the substantia nigra in our morphological analyses. Thus, the mouse dopaminergic neurons expressing UCH-L1^{I93M} may die prior to the formation of Lewy bodies, or those mice might form these structures at stages beyond the period of our study.

The mechanisms responsible for dopaminergic cell loss in the substantia nigra of H-hI93M mice remain elusive. The I93M mutation in UCH-L1 reduces its hydrolase activity by about 50%, which has been suggested as a cause for the pathogenesis of PD (Nishikawa et al., 2003). However, we have not found clear evidence for nigro-striatal dopaminergic pathology in gad mice (data not shown). Since expression of UCH-L1 is not detected in gad mice, the reduction of hydrolase activity alone would not be the cause of PD. In light of our finding here that transgenic expression of UCH-L1^{I93M} results in dopaminergic pathology in mice, it would seem that this mutation elicits a gain of toxic function leading to the neuronal toxicity in the substantia nigra.

Our previous work using circular dichroism suggests that the I93M mutation reduces the α-helical content of UCH-L1 (Nishikawa et al., 2003). Recently, we had also showed, using small-angle neutron scattering, that wild-type or I93M mutant UCH-L1 exists as a dimmer in an aqueous solution. Moreover, their configuration differed; wild-type UCH-L1 has ellipsoidal shape where as I93M mutant has more globular shape (Naito et al., 2006). Cells expressing UCH-L1^{I93M} are more prone to form inclusions (Ardley et al., 2004). Proteomic analysis of autopsied brains from PD patients and AD patients shows that UCH-L1 is extensively modified by carbonyl formation, methionine oxidation and cysteine oxidation in the diseased brains (Choi et al., 2004). These modifications are shown to result from oxidative stress (Choi et al., 2004). We show here that I93M mutation in UCH-L1 increases its insolubility *in vivo*. From the very limited expression of human UCH-L1 I93M, it is possible to speculate that endogenous mouse UCH-L1 might become insoluble in the presence of I93M UCH-L1. In addition, L-hI93M neurons were more susceptible than hWT or non-Tg neurons to MPTP, an inhibitor of complex I. This observation suggests that UCH-L1^{I93M} easily gains toxicity under oxidative stress. The conformational change and/or the additional methionine oxidation in UCH-L1 caused by I93M mutation may cause increased insolubility and lead to the gain of a toxic function.

In addition, our behavioral analysis revealed that H-hI93M mice exhibit very slight defects in spontaneous, voluntary movement, as shown by their hyperlocomotion at 11–13 weeks of age and by their hypolocomotion at 19–21 weeks of age in the home cage monitor test. Patients with PD exhibit no clinical symptoms until 70–80% of dopaminergic neurons are lost (Dauer and Przedborski, 2003). Thus, the level of dopaminergic neuronal loss seen in H-hI93M mice might not be sufficient to produce severe clinical phenotypes. It is difficult to explain the hyperlocomotion detected at 11–13 weeks of age, by simple changes in the nigro-striatal pathway. Other brain areas might be related to the locomotor changes seen in H-hI93M mice. We will need further analysis to connect the dopaminergic cell loss and defects in spontaneous, voluntary movement in H-hI93M mice.

In attempts to replicate neuropathological aspects of PD, several of the familial PD genes have been altered in mice. Up to date, α-synuclein Tg mice with or without mutation (Fernagut and Chesselet, 2004), parkin knockout mice (Goldberg et al., 2003; Itier et al., 2003; Palacino et al., 2004; Perez and Palmiter, 2005; Von Coelln et al., 2004), and DJ-1 knockout mice (Chen et al., 2005; Goldberg et al., 2005; Kim et al., 2005) have been reported. Although these mice show some alterations in the function of dopaminergic neurons, none has dopaminergic neuron loss in the substantia nigra. Thus, we have developed the first mouse model with an alteration in a familial PD gene that leads to dopaminergic cell loss. Further analysis of these mice will help establish the role of UCH-L1 in PD, which may elucidate a common pathway for both familial and sporadic PD.

Acknowledgements

References

Aoki, S., Su, Q., Li, H., Nishikawa, K., Ayukawa, K., Hara, Y., Namikawa, K., Kiryu-Seo, S., Kiyama, H., Wada, K., 2002. Identification of an axotomy-induced glycosylated protein, AIGP1, possibly involved in cell death triggered by endoplasmic reticulum-Golgi stress. J. Neurosci. 22, 10751–10760.

Ardley, H.C., Scott, G.B., Rose, S.A., Tan, N.G., Robinson, P.A., 2004. UCH-L1 aggresome formation in response to proteasome impairment indicates a role in inclusion formation in Parkinson's disease. J. Neurochem. 90, 379–391.

Bonifati, V., Rizzu, P., van Baren, M.J., Schaap, O., Breedveld, G.J., Krieger, E., Dekker, M.C., Squitieri, F., Ibanez, P., Joosse, M., van Dongen, J.W., Vanacore, N., van Swieten, J.C., Brice, A., Meco, G., van Duijn, C.M., Oostra, B.A., Heutink, P., 2003. Mutations in the DJ-1 gene associated with autosomal recessive early-onset parkinsonism. Science 299, 256–259.

Chartier-Harlin, M.C., Kachergus, J., Roumier, C., Mouroux, V., Douay, X., Lincoln, S., Levecque, C., Larvor, L., Andrieux, J., Hulihan, M., Waucquier, N., Defebvre, L., Amouyel, P., Farrer, M., Destee, A., 2004. Alpha-synuclein locus duplication as a cause of familial Parkinson's disease. Lancet 364, 1167–1169.

Chen, L., Cagniard, B., Mathews, T., Jones, S., Koh, H.C., Ding, Y., Carvey, P.M., Ling, Z., Kang, U.J., Zhuang, X., 2005. Age-dependent motor deficits and dopaminergic dysfunction in DJ-1 null mice. J. Biol. Chem. 280, 21418–21426.

Choi, J., Levey, A.I., Weintraub, S.T., Rees, H.D., Gearing, M., Chin, L.S., Li, L., 2004. Oxidative modifications and down-regulation of ubiquitin carboxyl-terminal hydrolase L1 associated with idiopathic Parkinson's and Alzheimer's diseases. J. Biol. Chem. 279, 13256–13264.

Dauer, W., Przedborski, S., 2003. Parkinson's disease: mechanisms and models. Neuron 39, 889–909.

Farrer, M., Kachergus, J., Forno, L., Lincoln, S., Wang, D.S., Hulihan, M., Maraganore, D., Gwinn-Hardy, K., Wszolek, Z., Dickson, D., Langston, J.W., 2004. Comparison of kindreds with parkinsonism and alpha-synuclein genomic multiplications. Ann. Neurol. 55, 174–179.

Fernagut, P.O., Chesselet, M.F., 2004. Alpha-synuclein and transgenic mouse models. Neurobiol. Dis. 17, 123–130.

Furuya, T., Hayakawa, H., Yamada, M., Yoshimi, K., Hisahara, S., Miura, M., Mizuno, Y., Mochizuki, H., 2004. Caspase-11 mediates inflammatory dopaminergic cell death in the 1-methyl-4-phenyl-1,2,3,6-tetrahydropyridine mouse model of Parkinson's disease. J. Neurosci. 24, 1865–1872.

Goldberg, M.S., Fleming, S.M., Palacino, J.J., Cepeda, C., Lam, H.A., Bhatnagar, A., Meloni, E.G., Wu, N., Ackerson, L.C., Klapstein, G.J., Gajendiran, M., Roth, B.L., Chesselet, M.F., Maidment, N.T., Levine, M.S., Shen, J., 2003. Parkin-deficient mice exhibit nigrostriatal deficits but not loss of dopaminergic neurons. J. Biol. Chem. 278, 43628–43635.

Goldberg, M.S., Pisani, A., Haburcak, M., Vortherms, T.A., Kitada, T., Costa, C., Tong, Y., Martella, G., Tscherter, A., Martins, A., Bernardi, G., Roth, B.L., Pothos, E.N., Calabresi, P., Shen, J., 2005. Nigrostriatal dopaminergic deficits and hypokinesia caused by inactivation of the familial Parkinsonism-linked gene DJ-1. Neuron 45, 489–496.

Hemelaar, J., Borodovsky, A., Kessler, B.M., Reverter, D., Cook, J., Kolli, N., Gan-Erdene, T., Wilkinson, K.D., Gill, G., Lima, C.D., Ploegh, H.L., Ovaa, H., 2004. Specific and covalent targeting of conjugating and deconjugating enzymes of ubiquitin-like proteins. Mol. Cell. Biol. 24, 84–95.

Hooper, D., Kawamura, M., Hoffman, B., Kopin, I.J., Hunyady, B., Mezey, E., Eisenhofer, G., 1997. Tyrosine hydroxylase assay for detection of low levels of enzyme activity in peripheral tissues. J. Chromatogr. B: Biomed. Sci. Appl. 694, 317–324.

Ibanez, P., Bonnet, A.M., Debarges, B., Lohmann, E., Tison, F., Pollak, P., Agid, Y., Durr, A., Brice, A., 2004. Causal relation between alpha-synuclein gene duplication and familial Parkinson's disease. Lancet 364, 1169–1171.

Itier, J.M., Ibanez, P., Mena, M.A., Abbas, N., Cohen-Salmon, C., Bohme, G.A., Laville, M., Pratt, J., Corti, O., Pradier, L., Ret, G., Joubert, C., Periquet, M., Araujo, F., Negroni, J., Casarejos, M.J., Canals, S., Solano, R., Serrano, A., Gallego, E., Sanchez, M., Denefle, P., Benavides, J., Tremp, G., Rooney, T.A., Brice, A., Garcia de Yebenes, J., 2003. Parkin gene inactivation alters behaviour and dopamine neurotransmission in the mouse. Hum. Mol. Genet. 12, 2277–2291.

Kahle, P.J., Neumann, M., Ozmen, L., Muller, V., Odoy, S., Okamoto, N., Jacobsen, H., Iwatsubo, T., Trojanowski, J.Q., Takahashi, H., Wakabayashi, K., Bogdanovic, N., Riederer, P., Kretzschmar, H.A., Haass, C., 2001. Selective insolubility of alpha-synuclein in human Lewy body diseases is recapitulated in a transgenic mouse model. Am. J. Pathol. 159, 2215–2225.

Kim, R.H., Smith, P.D., Aleyasin, H., Hayley, S., Mount, M.P., Pownall, S., Wakeham, A., You-Ten, A.J., Kalia, S.K., Horne, P., Westaway, D., Lozano,

A.M., Anisman, H., Park, D.S., Mak, T.W., 2005. Hypersensitivity of DJ-1-deficient mice to 1-methyl-4-phenyl-1,2,3,6-tetrahydropyridine (MPTP) and oxidative stress. Proc. Natl. Acad. Sci. U.S.A. 102, 5215–5220.

Kitada, T., Asakawa, S., Hattori, N., Matsumine, H., Yamamura, Y., Minoshima, S., Yokochi, M., Mizuno, Y., Shimizu, N., 1998. Mutations in the parkin gene cause autosomal recessive juvenile parkinsonism. Nature 392, 605–608.

Kruger, R., Kuhn, W., Muller, T., Woitalla, D., Graeber, M., Kosel, S., Przuntek, H., Epplen, J.T., Schols, L., Riess, O., 1998. Ala30Pro mutation in the gene encoding alpha-synuclein in Parkinson's disease. Nat. Genet. 18, 106–108.

Larsen, C.N., Krantz, B.A., Wilkinson, K.D., 1998. Substrate specificity of deubiquitinating enzymes: ubiquitin C-terminal hydrolases. Biochemistry 37, 3358–3368.

Leroy, E., Boyer, R., Auburger, G., Leube, B., Ulm, G., Mezey, E., Harta, G., Brownstein, M.J., Jonnalagada, S., Chernova, T., Dehejia, A., Lavedan, C., Gasser, T., Steinbach, P.J., Wilkinson, K.D., Polymeropoulos, M.H., 1998. The ubiquitin pathway in Parkinson's disease. Nature 395, 451–452.

Lincoln, S., Vaughan, J., Wood, N., Baker, M., Adamson, J., Gwinn-Hardy, K., Lynch, T., Hardy, J., Farrer, M., 1999. Low frequency of pathogenic mutations in the ubiquitin carboxy-terminal hydrolase gene in familial Parkinson's disease. Neuroreport 10, 427–429.

Liu, Y., Fallon, L., Lashuel, H.A., Liu, Z., Lansbury Jr., P.T., 2002. The UCH-L1 gene encodes two opposing enzymatic activities that affect alpha-synuclein degradation and Parkinson's disease susceptibility. Cell 111, 209–218.

Lo Bianco, C., Schneider, B.L., Bauer, M., Sajadi, A., Brice, A., Iwatsubo, T., Aebischer, P., 2004. Lentiviral vector delivery of parkin prevents dopaminergic degeneration in an alpha-synuclein rat model of Parkinson's disease. Proc. Natl. Acad. Sci. U.S.A. 101, 17510–17515.

Lowe, J., McDermott, H., Landon, M., Mayer, R.J., Wilkinson, K.D., 1990. Ubiquitin carboxyl-terminal hydrolase (PGP 9.5) is selectively present in ubiquitinated inclusion bodies characteristic of human neurodegenerative diseases. J. Pathol. 161, 153–160.

Maraganore, D.M., Farrer, M.J., Hardy, J.A., Lincoln, S.J., McDonnell, S.K., Rocca, W.A., 1999. Case-control study of the ubiquitin carboxy-terminal hydrolase L1 gene in Parkinson's disease. Neurology 53, 1858–1860.

Mochizuki, H., Hayakawa, H., Migita, M., Shibata, M., Tanaka, R., Suzuki, A., Shimo-Nakanishi, Y., Urabe, T., Yamada, M., Tamayose, K., Shimada, T., Miura, M., Mizuno, Y., 2001. An AAV-derived Apaf-1 dominant negative inhibitor prevents MPTP toxicity as antiapoptotic gene therapy for Parkinson's disease. Proc. Natl. Acad. Sci. U.S.A. 98, 10918–10923.

Naito, S., Mochizuki, H., Yasuda, T., Mizuno, Y., Furusaka, M., Ikeda, S., Adachi, T., Shimizu, H.M., Suzuki, J., Fujiwara, S., Okada, T., Nishikawa, K., Aoki, S., Wada, K., 2006. Characterization of multimetric variants of ubiquitin carboxyl-terminal hydrolase L1 in water by small-angle neutron scattering. Biochem. Biophys. Res. Commun. 339, 717–725.

Naoi, M., Takahashi, T., Nagatsu, T., 1988. Simple assay procedure for tyrosine hydroxylase activity by high-performance liquid chromatography employing coulometric detection with minimal sample preparation. J. Chromatogr. 427, 229–238.

Nishikawa, K., Li, H., Kawamura, R., Osaka, H., Wang, Y.L., Hara, Y., Hirokawa, T., Manago, Y., Amano, T., Noda, M., Aoki, S., Wada, K., 2003. Alterations of structure and hydrolase activity of parkinsonism-associated human ubiquitin carboxyl-terminal hydrolase L1 variants. Biochem. Biophys. Res. Commun. 304, 176–183.

Osaka, H., Wang, Y.L., Takada, K., Takizawa, S., Setsuie, R., Li, H., Sato, Y., Nishikawa, K., Sun, Y.J., Sakurai, M., Harada, T., Hara, Y., Kimura, I., Chiba, S., Namikawa, K., Kiyama, H., Noda, M., Aoki, S., Wada, K., 2003. Ubiquitin carboxy-terminal hydrolase L1 binds to and stabilizes mono-ubiquitin in neuron. Hum. Mol. Genet. 12, 1945–1958.

Paisan-Ruiz, C., Jain, S., Evans, E.W., Gilks, W.P., Simon, J., van der Brug, M., Lopez de Munain, A., Aparicio, S., Gil, A.M., Khan, N., Johnson, J., Martinez, J.R., Nicholl, D., Carrera, I.M., Pena, A.S., de Silva, R., Lees, A., Marti-Masso, J.F., Perez-Tur, J., Wood, N.W., Singleton, A.B., 2004. Cloning of the gene containing mutations that cause PARK8-linked Parkinson's disease. Neuron 44, 595–600.

Palacino, J.J., Sagi, D., Goldberg, M.S., Krauss, S., Motz, C., Wacker, M., Klose, J., Shen, J., 2004. Mitochondrial dysfunction and oxidative damage in parkin-deficient mice. J. Biol. Chem. 279, 18614–18622.

Perez, F.A., Palmiter, R.D., 2005. Parkin-deficient mice are not a robust model of parkinsonism. Proc. Natl. Acad. Sci. U.S.A. 102, 2174–2179.

Polymeropoulos, M.H., Lavedan, C., Leroy, E., Ide, S.E., Dehejia, A., Dutra, A., Pike, B., Root, H., Rubenstein, J., Boyer, R., Stenroos, E.S., Chandrasekharappa, S., Athanassiadou, A., Papapetropoulos, T., Johnson, W.G., Lazzarini, A.M., Duvoisin, R.C., Di Iorio, G., Golbe, L.I., Nussbaum, R.L., 1997. Mutation in the alpha-synuclein gene identified in families with Parkinson's disease. Science 276, 2045–2047.

Rane, N.S., Yonkovich, J.L., Hegde, R.S., 2004. Protection from cytosolic prion protein toxicity by modulation of protein translocation. EMBO J. 23, 4550–4559.

Saigoh, K., Wang, Y.L., Suh, J.G., Yamanishi, T., Sakai, Y., Kiyosawa, H., Harada, T., Ichihara, N., Wakana, S., Kikuchi, T., Wada, K., 1999. Intragenic deletion in the gene encoding ubiquitin carboxy-terminal hydrolase in gad mice. Nat. Genet. 23, 47–51.

Sandmann-Keil, D., Braak, H., Okochi, M., Haass, C., Braak, E., 1999. Alpha-synuclein immunoreactive Lewy bodies and Lewy neurites in Parkinson's disease are detectable by an advanced silver-staining technique. Acta Neuropathol. (Berl.) 98, 461–464.

Sasahara, M., Fries, J.W., Raines, E.W., Gown, A.M., Westrum, L.E., Frosch, M.P., Bonthron, D.T., Ross, R., Collins, T., 1991. PDGF B-chain in neurons of the central nervous system, posterior pituitary, and in a transgenic model. Cell 64, 217–227.

Singleton, A.B., Farrer, M., Johnson, J., Singleton, A., Hague, S., Kachergus, J., Hulihan, M., Peuralinna, T., Dutra, A., Nussbaum, R., Lincoln, S., Crawley, A., Hanson, M., Maraganore, D., Adler, C., Cookson, M.R., Muenter, M., Baptista, M., Miller, D., Blancato, J., Hardy, J., Gwinn-Hardy, K., 2003. Alpha-synuclein locus triplication causes Parkinson's disease. Science 302, 841.

Uchihara, T., Nakamura, A., Mochizuki, Y., Hayashi, M., Orimo, S., Isozaki, E., Mizutani, T., 2005. Silver stainings distinguish Lewy bodies and glial cytoplasmic inclusions: comparison between Gallyas-Braak and Campbell-Switzer methods. Acta Neuropathol. (Berl.) 110, 255–260.

Valente, E.M., Abou-Sleiman, P.M., Caputo, V., Muqit, M.M., Harvey, K., Gispert, S., Ali, Z., Del Turco, D., Bentivoglio, A.R., Healy, D.G., Albanese, A., Nussbaum, R., Gonzalez-Maldonado, R., Deller, T., Salvi, S., Cortelli, P., Gilks, W.P., Latchman, D.S., Harvey, R.J., Dallapiccola, B., Auburger, G., Wood, N.W., 2004. Hereditary early-onset Parkinson's disease caused by mutations in PINK1. Science 304, 1158–1160.

Vila, M., Przedborski, S., 2004. Genetic clues to the pathogenesis of Parkinson's disease. Nat. Med. 10 (Suppl.), S58–S62.

Von Coelln, R., Thomas, B., Savitt, J.M., Lim, K.L., Sasaki, M., Hess, E.J., Dawson, V.L., Dawson, T.M., 2004. Loss of locus coeruleus neurons and reduced startle in parkin null mice. Proc. Natl. Acad. Sci. U.S.A. 101, 10744–10749.

Wang, Y.L., Liu, W., Sun, Y.J., Kwon, J., Setsuie, R., Osaka, H., Noda, M., Aoki, S., Yoshikawa, Y., Wada, K., 2006. Overexpression of ubiquitin carboxyl-terminal hydrolase L1 arrests spermatogenesis in transgenic mice. Mol. Reprod. Develop. 73, 40–49.

Wang, Y.L., Takeda, A., Osaka, H., Hara, Y., Furuta, A., Setsuie, R., Sun, Y.J., Kwon, J., Sato, Y., Sakurai, M., Noda, M., Yoshikawa, Y., Wada, K., 2004. Accumulation of beta- and gamma-synucleins in the ubiquitin carboxyl-terminal hydrolase L1-deficient gad mouse. Brain Res. 1019, 1–9.

Watanabe, I., Vachal, E., Tomita, T., 1977. Dense core vesicles around the Lewy body in incidental Parkinson's disease: an electron microscopic study. Acta Neuropathol. (Berl.) 39, 173–175.

Wilkinson, K.D., Lee, K.M., Deshpande, S., Duerksen-Hughes, P., Boss, J.M., Pohl, J., 1989. The neuron-specific protein PGP 9.5 is a ubiquitin carboxyl-terminal hydrolase. Science 246, 670–673.

Zimprich, A., Biskup, S., Leitner, P., Lichtner, P., Farrer, M., Lincoln, S., Kachergus, J., Hulihan, M., Uitti, R.J., Calne, D.B., Stoessl, A.J., Pfeiffer, R.F., Patenge, N., Carbajal, I.C., Vieregge, P., Asmus, F., Muller-Minsk, B., Dickson, D.W., Meeting, T., Strom, T.M., Wszolek, Z.K., Gasser, T., 2004. Mutations in LRRK2 cause autosomal-dominant parkinsonism with allomorphic pathology. Neurone 44, 601–607.

Cell Injury, Repair, Aging and Apoptosis

Photoreceptor Cell Apoptosis in the Retinal Degeneration of *Uchl3*-Deficient Mice

Yae Sano,*[†] Akiko Furuta,* Rieko Setsuie,*[†]
Hisae Kikuchi,* Yu-Lai Wang,* Mikako Sakurai,*[†]
Jungkee Kwon,*[‡] Mami Noda,[†] and Keiji Wada*

*From the Department of Degenerative Neurological Diseases,**
National Institute of Neuroscience, National Center of Neurology
and Psychiatry, Tokyo, Japan; the Laboratory of
Pathophysiology,[†] Graduate School of Pharmaceutical Sciences,
Kyushu University, Fukuoka, Japan; and the Laboratory of
Animal Medicine,[‡] College of Veterinary Medicine, Chonbuk
National University, Jeonju, Korea

UCH-L3 belongs to the ubiquitin C-terminal hydrolase family that deubiquitinates ubiquitin-protein conjugates in the ubiquitin-proteasome system. A murine *Uchl3* deletion mutant displays retinal degeneration, muscular degeneration, and mild growth retardation. To elucidate the function of UCH-L3, we investigated histopathological changes and expression of apoptosis- and oxidative stress-related proteins during retinal degeneration. In the normal retina, UCH-L3 was enriched in the photoreceptor inner segment that contains abundant mitochondria. Although the retina of *Uchl3*-deficient mice showed no significant morphological abnormalities during retinal development, prominent retinal degeneration became manifested after 3 weeks of age associated with photoreceptor cell apoptosis. Ultrastructurally, a decreased area of mitochondrial cristae and vacuolar changes were observed in the degenerated inner segment. Increased immunoreactivities for manganese superoxide dismutase, cytochrome *c* oxidase I, and apoptosis-inducing factor in the inner segment indicated mitochondrial oxidative stress. Expression of cytochrome c, caspase-1, and cleaved caspase-3 did not differ between wild-type and mutant mice; however, immunoreactivity for endonuclease G was found in the photoreceptor nuclei in the mutant retina. Hence, loss of UCH-L3 leads to mitochondrial oxidative stress-related photoreceptor cell apoptosis in a caspase-independent manner. Thus, *Uchl3*-deficient mice represent a model for adult-onset retinal degeneration associated with mito-
chondrial impairment. *(Am J Pathol 2006, 169:132–141; DOI: 10.2353/ajpath.2006.060085)*

The ubiquitin system has been implicated in numerous cellular processes, including protein quality control, cell cycle, cell proliferation, signal transduction, membrane protein internalization, and apoptosis.[1,2] Ubiquitin-dependent processes are regulated by ubiquitinating enzymes, E1, E2, and E3, and deubiquitinating enzymes such as ubiquitin-specific proteases and ubiquitin C-terminal hydrolases (UCHs).[1,3–5] To date, four isozymes of UCHs, UCH-L1, UCH-L3, UCH-L4, and UCH-L5, have been cloned in mouse or human.[6–8] UCH-L1, also known as PGP 9.5, has been well characterized among the isozymes. UCH-L1 is selectively localized to brains and testis/ovaries[7] and functions as a ubiquitin ligase in addition to a deubiquitinating enzyme.[9] Furthermore, two distinct mutations are linked to Parkinson's disease in human[10] and gracile axonal dystrophy (*gad*) in mice.[11] UCH-L3, on the other hand, displays 52% amino acid identity to UCH-L1.[12] Uchl3 mRNA is expressed throughout various tissues and is especially enriched in testis and thymus.[13] In addition to its ubiquitin hydrolase activity, *in vitro* studies indicate that UCH-L3 cleaves the C terminus of the ubiquitin-like protein Nedd-8.[14,15] Although UCH-L1 and UCH-L3 are suggested to function as reciprocal modulators of germ cell apoptosis in experimental cryptorchid testis,[16] the cellular localization and function of UCH-L3 remain unknown in other organs.

Recently, *Uchl3*-deficient mice were generated with a deletion of exons 3 to 7, which are essential for hydrolase

132

activity.[13] These mutant mice display postnatal retinal and muscular degenerations as well as mild growth retardation.[17] Retinal development is morphologically normal, but progressive retinal degeneration is reported to be evident at 3 months after birth.[17] However, precise chronological changes and the mechanism of the retinal degeneration in *Uchl3*-deficient mice has not been studied.

Both the caspase-dependent pathway and the caspase-independent pathway have been proposed to be involved in the models of retinal degeneration, including model animals for retinitis pigmentosa (such as Royal College of Surgeons (RCS) rat and retinal degeneration (*rd*) mice),[18] retinal detachment,[19] light injury,[20,21] ischemic injury,[22] and age-related macular degeneration.[23] In the ubiquitin system, UCH-L1 is involved in ischemia-induced apoptosis in the inner retina.[24] The role of UCH-L3 in retinal degeneration, however, is unclear.

To elucidate the function of UCH-L3, we investigated the histopathological changes and protein expression with respect to apoptotic pathways in *Uchl3*-deficient mice. Our results show that UCH-L3 is mainly localized to the photoreceptor inner segment that contains abundant mitochondria in the normal retina. *Uchl3*-deficient mice displayed caspase-independent apoptosis during postnatal retinal degeneration associated with increased expression of the markers for mitochondrial oxidative stress at the inner segment. We propose a possible antiapoptotic role of UCH-L3 in photoreceptor cells.

Materials and Methods

Animals

We used age-matched *Uchl3*-deficient mice and wild-type mice, all of which were offspring male from 15 to 20 pairs of heterozygotes that had been backcrossed with C57BL/6J at postnatal ages of 0 days (P0), 10 days (P10), 3 weeks (3w), 6 weeks (6w), 8 weeks (8w), and 12 weeks (12w). The total number of wild-type and *Uchl3*-deficient mice examined in the present study was 79, of which 30 mice were used for Western blotting, 42 mice were used for hematoxylin and eosin staining, immunohistochemistry, and terminal deoxynucleotidyl transferase-mediated dUTP nick end labeling (TUNEL) assay, and 7 mice were used for electron microscopy. The mice were maintained at the National Institute of Neuroscience, National Center of Neurology and Psychiatry (Tokyo, Japan). The experiments using the mice were approved by the Institute's Animal Investigation Committee.

Western Blotting

Eyes from P10-, 3w-, and 6w-old mice of both genotypes (10 mice in each time point, for a total of 30 mice) were lysed in protein lysis buffer (100 mmol/L Tris-HCl, pH 8.0, 300 mmol/L NaCl, 2% Triton X-100, 0.2% SDS, 2% sodium deoxycholate, 2 mmol/L EDTA) containing protease inhibitor (Complete protease inhibitor cocktail; Sigma-Aldrich, St. Louis, MO). The amount of total protein of each sample was determined by the Bio-Rad protein assay (Bio-Rad, Hercules, CA) using bovine serum albumin as a standard. Total protein (50 μg/lane) was separated by 15% SDS-polyacrylamide gels (Perfect NT Gel, DRC, Tokyo, Japan). Proteins were transferred to immuno-Blot polyvinylidene difluoride membranes (Bio-Rad) and incubated with 5% skim milk in TBST (50 mmol/L Tris-HCl-buffered saline, pH 7.0, containing 0.05% Triton X-100) for 1 hour at room temperature. The membranes were incubated with a 1:1000 dilution of each primary antibody for UCH-L1, UCH-L3,[25] and β-actin (1:1000; Sigma-Aldrich) overnight at 4°C. For the preparation of anti-mouse UCH-L1 antibody, histidine-tagged mouse UCH-L1 (6His-mUCH-L1) was prepared as described previously[26] and used to generate a polyclonal antiserum in rabbit (Takara, Tokushima, Japan). The polyclonal antibody was purified by affinity chromatography. The specificity of this antibody to the mouse UCH-L1 was verified by Western blotting using brain lysates from *gad* mice and wild-type mice (data not shown). The membranes were washed in TBST and further incubated with antimouse or rabbit IgG-horseradish peroxidase conjugate (1:1000; Chemicon, Temecula, CA). After washing in TBST, the membranes were developed with the Super Signal West Dura or Femto Extended Duration Substrate (Pierce, Rockford, IL) and analyzed with a ChemiImager (Alpha Innotech, San Leandro, CA). Western blotting was performed five times per each antibody.

Morphometric Analysis and Immunohistochemistry of Retina

Mice of both genotypes at P0, P10, 3w, 6w, 8w, and 12w of age (7 mice in each time point, total of 42 mice) were deeply anesthetized with diethylether, decapitated, and the eyes removed, immersion-fixed with 4% paraformaldehyde overnight at 4°C, and embedded in paraffin wax. Deparaffinized sections were stained with hematoxylin and eosin and examined under an Axioplan2 microscope (Carl Zeiss, Oberkochen, Germany) at a magnification ×400, and the thickness of each layer was measured using WinRoof software (Mitani Shoji, Tokyo, Japan).

For immunohistochemical studies, 5-μm-thick sagittal sections at the level of the optic nerve were deparaffinized and treated with 1% hydrogen peroxide (H_2O_2) for 30 minutes, incubated with 1% skim milk in phosphate-buffered saline (PBS, pH 7.4) for 1 hour at room temperature followed by incubation overnight at 4°C with each primary antibody for UCH-L1 and UCH-L3[25] diluted 1:500 in 1% skim milk in PBS. To characterize apoptosis- and oxidative stress-related proteins, antibodies to the following proteins were used; apoptosis-inducing factor (AIF; 1:500, Chemicon), caspase-1 (1:100; Cell Signaling Technology, Beverly, MA), caspase-3 (1:1000; Cell Signaling Technology), cleaved caspase-3 (1:50; Cell Signaling Technology), cytochrome *c* (1:1000; Santa Cruz Biotechnology, Santa Cruz, CA), cytochrome *c* oxidase I

(COX, 1:10,000; Molecular Probes, Eugene, OR), endonuclease G (Endo G; 1:500, Chemicon) and manganese superoxide dismutase (Mn-SOD; 1:10,000, Stressgen, Victoria, BC, Canada). The sections were washed in PBS and then incubated with biotinylated secondary antibodies diluted 1:500 in PBS containing 1% skim milk. The sections were treated with the VECTASTAIN Elite ABC kit (Vector Laboratories, Burlingame, CA) according to the manufacturer's protocol and developed with 0.02% 3,3′-diaminobenzidine tetrahydrochloride solution containing 0.003% H_2O_2. After visualization, sections were counterstained with hematoxylin. Sections were examined with an Axioplan2 microscope (Carl Zeiss). Immunohistochemistry was performed in at least three repeated experiments. The relative immunoreactivity for COX, Mn-SOD, AIF, and Endo G in each layer of mutant mice was compared with that of wild-type mice and was classified into no change (−), slight increase (±), mild increase (+), and marked increase (++).

TUNEL Staining

Apoptotic cells were examined in mice of both genotypes at P0, P10, 3w, 6w, 8w, and 12w (7 mice in each time point, for a total of 42 mice) by TUNEL stain using the Dead-End Fluorimetric TUNEL system kit (Promega, Madison, WI) according to the manufacturer's instructions. The sections were examined by using a confocal laser scanning microscope (Olympus, Tokyo, Japan). The microphotographs were captured at magnification ×400 (0.066 mm^2/each retinal section), positive cells were counted (Fluoview 2.0; Olympus), and the data were subjected to statistical analysis.

Electron Microscopic Analysis

3w-old mice of both genotypes (total 7 mice) were deeply anesthetized with 20% chloral hydrate aqueous solution and perfused with the following fixative: 2% paraformaldehyde, 2% glutaraldehyde in PBS, or sodium cacodylate buffer (pH 7.4). The eyes were removed and postfixed with the same fixative overnight at 4°C. The posterior segments of eyes were trimmed and washed with PBS or sodium cacodylate buffer, incubated in phosphate-buffered 1% osmium tetroxide for 1 hour, and dehydrated in ethanol and embedded in Epon 812 resin (TAAB, Berks, UK). Ultrathin sections (75 nm) were mounted on copper grids and stained with uranium acetate and lead citrate. The sections were observed using an H-7000 electron microscope (Hitachi, Tokyo, Japan). Morphometric analysis of mitochondria was performed by measuring average percentage of area occupied by cristae within a mitochondrion at the inner segment.

Statistical Analysis

In statistical analysis of thickness of retinal layers and TUNEL-positive cells, three wild-type and four *Uchl3*-deficient mice were used in each time point (P0, P10, 3w,
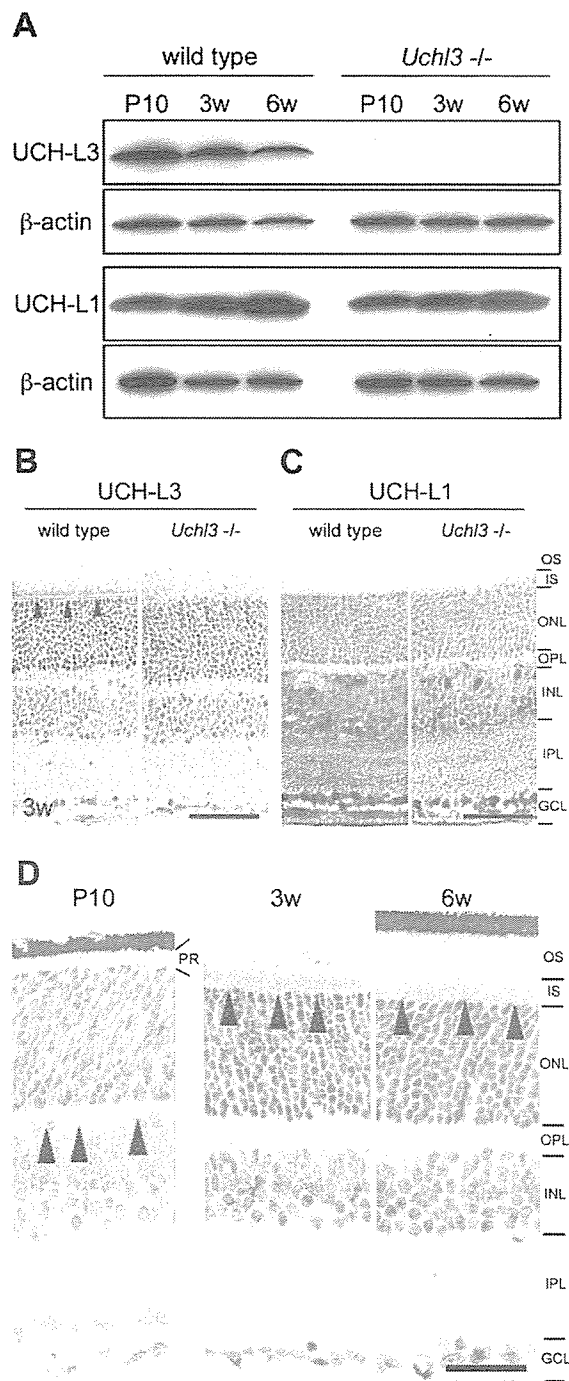

Figure 1. Expression of UCH-L1 and UCH-L3 in the retina of wild-type and *Uchl3*-deficient mice. A: Western blot analysis of UCH-L3 and UCH-L1 using whole-eye lysates from wild-type and *Uchl3*-deficient mice at P10, 3w, and 6w. The immunoreactive band for UCH-L3 is undetectable in *Uchl3*-deficient mice. Expression of UCH-L1 is similar between both genotypes. B and C: Immunohistochemistry for UCH-L3 (B) and UCH-L1 (C) in wild-type and *Uchl3*-deficient mice retinae at 3w. Immunoreactivity of UCH-L3 is found at the inner segment of the wild-type retina (arrowheads), whereas there is no significant immunoreactivity in *Uchl3*-deficient mice (B). UCH-L1 is expressed at the inner retina in both genotypes. D: Immunohistochemistry of UCH-L3 at P10, 3w, and 6w in wild-type retinae. UCH-L3 is faintly expressed in the outer plexiform layer at P10 (arrowheads). Thereafter, immunoreactivity for UCH-L3 is found in inner segment at 3w and 6w (arrowheads). PR, photoreceptor; OS, outer segment; IS, inner segment; ONL, outer nuclear layer; OPL, outer plexiform layer; INL, inner nuclear layer; IPL, inner plexiform layer; GCL, ganglion cell layer. Scale bars = 50 μm (B and C) and 20 μm (D).
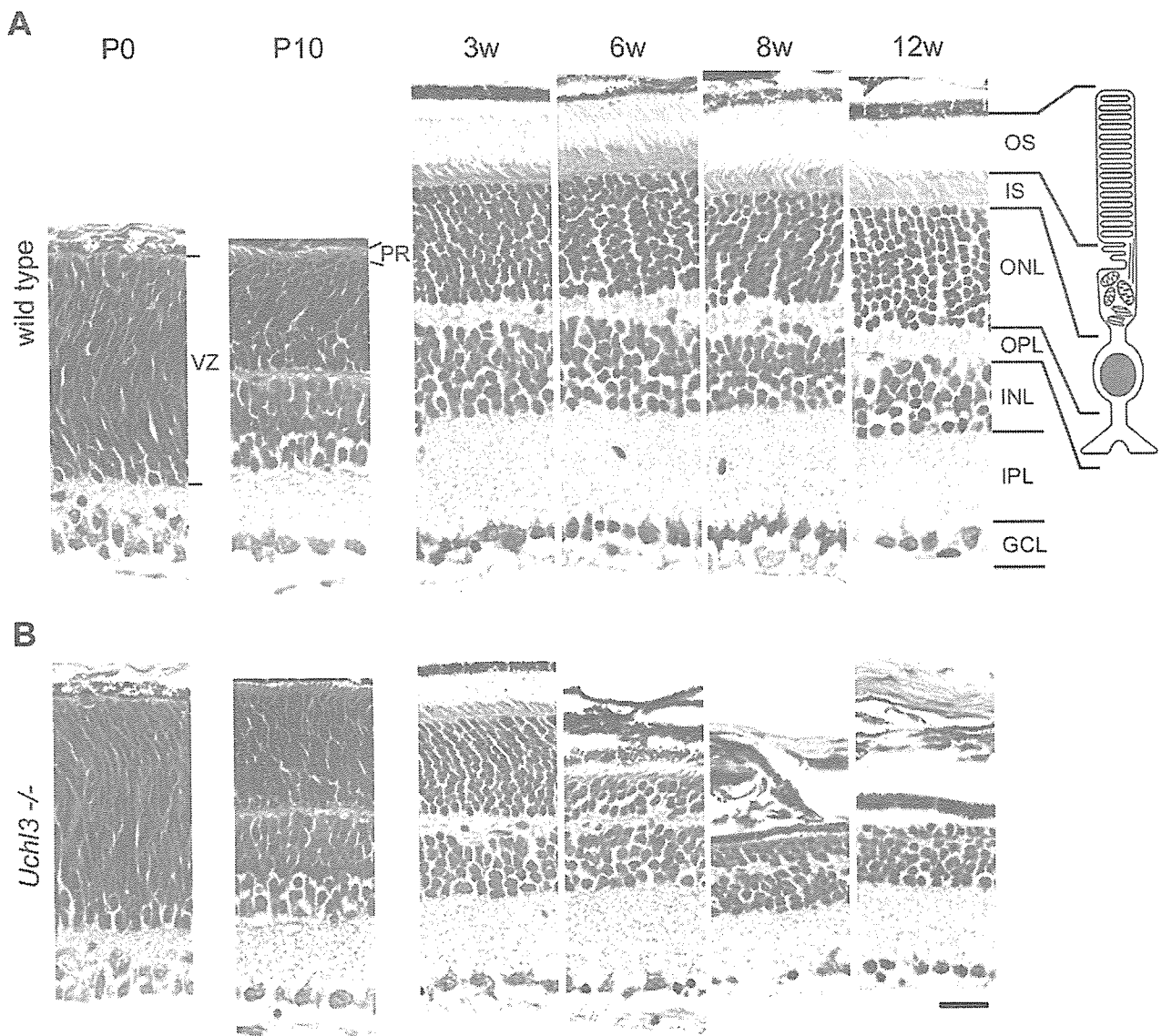
A

| PO | P10 | 3w | 6w | 8w | 12w |

B

Figure 2. Histopathological changes of postnatal development in wild-type (A) and retinal degeneration of *Uchl3*-deficient mice (B) at P0, P10, 3w, 6w, 8w, and 12w. There is no morphological difference between both genotypes at P0 and P10, whereas outer and inner segments, outer nuclear layers, and outer plexiform layers are progressively degenerated after 3w of age. The illustration indicates a rod photoreceptor cell. VZ, ventricular zone; PR, photoreceptor; OS, outer segment; IS, inner segment; ONL, outer nuclear layer; OPL, outer plexiform layer; INL, inner nuclear layer; IPL, inner plexiform layer; GCL, ganglion cell layer. H&E staining. Scale bar = 20 μm (A and B).

6w, 8w, and 12w; for a total of 42 mice). The percentage of cristae area to whole mitochondrion in ultramicrophotographs was measured in 50 mitochondria of each genotype from three wild-type mice and four *Uchl3*-deficient mice, and the data were subjected to statistical analysis. All statistical analyses were carried out by Student's *t*-test using Microsoft Excel.

Results

Expression of UCH-L3 in the Murine Retina

Western blotting detected UCH-L3 (~30 kd) in extracts of eyes from wild-type mice at P10, 3w, and 6w, but the band was undetectable in *Uchl3*-deficient mice (Figure

1A). The expression level of UCH-L1 was similar in both genotypes. There was a tendency that the level of UCH-L3 decreased with age while the level of UCH-L1 increased with age in wild-type mice of all samples examined (five blots per antibody). Immunohistochemically, the cellular distribution of UCH-L3 differed from that of UCH-L1. UCH-L3 was enriched in the photoreceptor inner segment in wild-type mice at 3w of age (Figure 1B), whereas UCH-L1 was expressed in both genotypes in the inner retina, which consists of the inner nuclear layer, inner plexiform layer, and ganglion cell layer (Figure 1C). Localization of UCH-L3 in the wild-type retina was altered with age (Figure 1D). Immunoreactivity for UCH-L3 was not found at P0. UCH-L3 was faintly expressed in the outer plexiform layer at P10. Thereafter, it was localized to

inner segment at 3w. The inner segment was less immu-
noreactive for UCH-L3 at 6w, 8w, and 12w, compared
with 3w.

Histopathological Changes of Retinal Degeneration in the Uchl3-Deficient Mice

Microscopic examination of retinal cross-sections re-
vealed no obvious histopathological changes during
early postnatal development at P0 and P10 in the retina of
Uchl3-deficient mice (Figure 2). At 3w of age, the mutant
retina began to degenerate in the inner segment and
ultimately disappeared at 12w (Figures 2B and 3D).
Thickness of the outer segment, outer nuclear layer, and
outer plexiform layer was also significantly decreased in
the mutant mice at 6w of age (Figure 3, C, E, and F).
Despite the conspicuous change in the photoreceptor
cells, the thickness of the mutant inner retina up to 12w of
age was not altered compared with that of the wild-type
(Figure 3, G–I).

Ultrastructurally, vacuolar changes were found in the
inner segment of Uchl3-deficient mice at 3w of age (Fig-
ure 4). Mitochondria at the inner segment of mutant mice
were slightly swollen. Groups of small round-to-oval
structures were observed in the degenerated inner seg-
ment (Figure 4D), and these structures were considered
to be the cross-sections of cell processes. Chromatin
condensation in photoreceptor nuclei was sometimes
seen in the outer nuclear layer at 3w (Figure 4F). Mor-
phometric analysis showed that the percentage of cristae
area to whole area of mitochondrion in the inner segment
of Uchl3-deficient mice was significantly lower than that of
wild-type mice (Figure 4, G and H).

Altered Expressions of Apoptosis-Related Proteins in the Degenerated Retina

Apoptotic cells in the retinal cross-sections were identi-
fied using the TUNEL staining. TUNEL-positive cells were
identified in the ventricular zone at P0 and inner nuclear
layer at P10 of both genotypes during the developmental
period (Figure 5, A and C). The number of TUNEL-posi-
tive cells slightly increased in the inner nuclear layer at
P10. After 3w of age, TUNEL-positive cells of mutant
retina significantly increased at the outer nuclear layer of
the mutant retina at 3w, 6w, and 8w (Figure 5, A and D).

To determine which apoptotic pathway was activated
in Uchl3-deficient mice, we examined immunoreactivities
of apoptosis-related proteins. Expression of cytochrome
c, caspase-3, and cleaved caspase-3 and caspase-1,
essential molecules for the caspase-dependent pathway,
were unchanged in both genotypes (Figure 6A), whereas
oxidative stress markers, COX and Mn-SOD as well as
AIF and Endo G, indicators of the caspase-independent
pathway, were altered in the mutant retina (Figure 6B).
Chronological changes in expression of markers for oxi-
dative stress and caspase-independent apoptosis at P0,
P10, 3w, 6w, 8w, and 12w are shown in Table 1. The
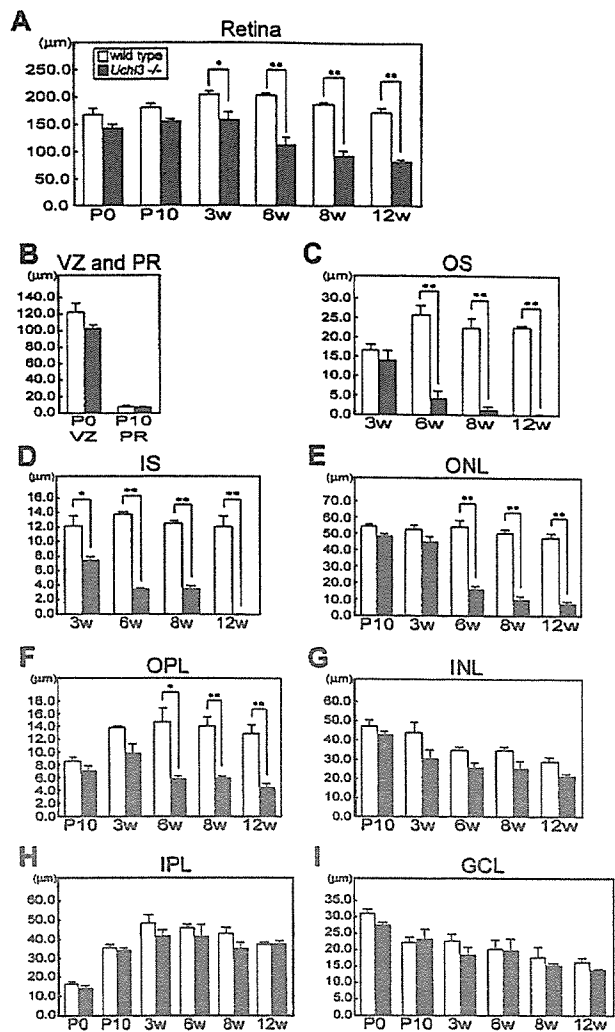immunoreactivity of COX was increased in the inner seg-

Figure 3. Chronological changes of retinal degeneration as assessed by
thickness of each layer at different ages in wild-type and *Uchl3*-deficient
mice. A: Total retinal thickness is progressively decreased after 3w of age. B:
Thickness of ventricular zone at P0 and photoreceptor layer at P10 shows no
significant changes between both genotypes. C–F: Thickness of outer retinal
layers in wild-type and *Uchl3*-deficient mice at different ages. The earliest
change is revealed at 3w of age in inner segment of mutant retina (D).
Thickness of outer segment (C), outer nuclear layer (E), and outer plexiform
layer (F) in *Uchl3*-deficient mice is significantly decreased with age com-
pared with that in the wild-type. G–I: Thickness of inner retinal layers in
wild-type and *Uchl3*-deficient mice at different ages. Thickness of inner
nuclear layer (G), inner plexiform layer (H), and ganglion cell layer (I) are
unchanged between both genotypes. Each value represents the mean ± SE
(*P < 0.05; **P < 0.01). In all panels, the white bars represent the thickness
in wild-type mice and the black bars represent the thickness in *Uchl3*-
deficient mice. VZ, ventricular zone; PR, photoreceptor; OS, outer segment;
IS, inner segment; ONL, outer nuclear layer; OPL, outer plexiform layer; INL,
inner nuclear layer; IPL, inner plexiform layer; GCL, ganglion cell layer.

ment at 3w and 6w. Mn-SOD was mildly increased in the
inner segment at 3w, 6w, and 8w. Although AIF was
enriched in the inner segment of Uchl3-deficient mice at
3w and 6w, nuclear labeling of AIF was not observed. On
the other hand, Endo G was localized to the nuclei of the
outer nuclear layer of the mutant retina at 3w and 6w.
Expression of Endo G was slightly increased in the outer
plexiform layer, inner nuclear layer, and inner plexiform
layer of Uchl3-deficient mice after 3w of age (Table 1).
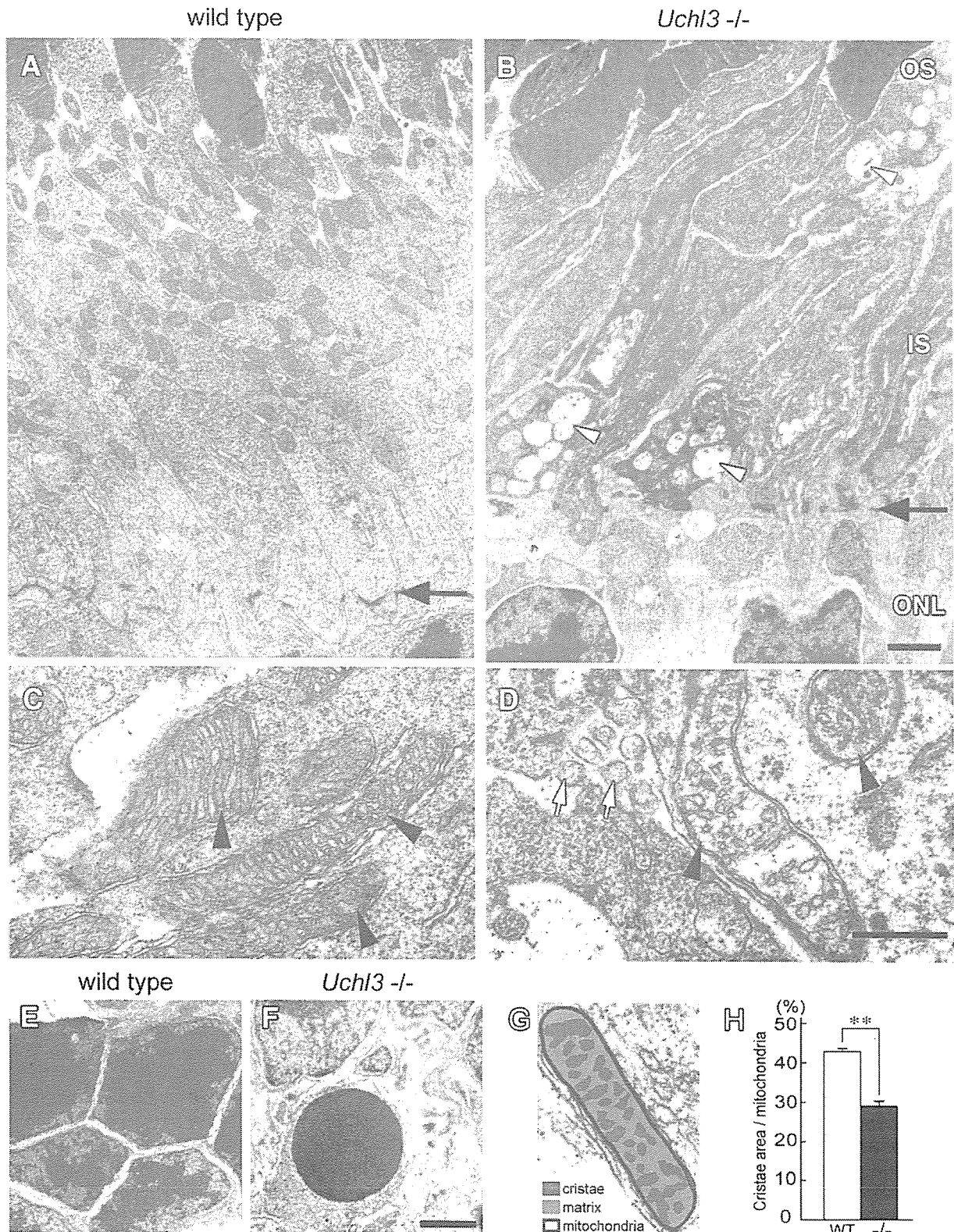Thus, degeneration of photoreceptor cells in Uchl3-defi-

Figure 4. Ultrastructure of the outer retina in wild-type (A, C, and E) and *Uchl3*-deficient mice (B, D, and F) at 3w of age. A and B: Inner segment of mutant retina is shrunken associated with vacuolar changes (**arrowheads** in B). **Arrows** in A and B indicate outer limiting membrane. C and D: Subsets of mitochondria at the inner segment in *Uchl3*-deficient mice are swollen with decreased cristae (**arrowheads** in D) compared with that of wild-type (**arrowheads** in C). Groups of small round-to-oval shaped structures are occasionally seen in degenerated inner segment (**white arrows** in D). E and F: Outer nuclear layer of wild-type (E) and *Uchl3*-deficient (F) mice. Chromatin condensation of photoreceptor cells is observed in mutant mice (F). G and H: Morphometric analysis of mitochondria was performed with the percentage of cristae area (G; red) against mitochondrial area (*n* = 50 for each genotype). Cristae area in the inner segment is significantly decreased in mutant retina (H, −/−, **black bar**) compared with that in wild-type (H, WT, **white bar**). Each value represents the mean ± SE (**$P < 0.01$). OS, outer segment; IS, inner segment; ONL, outer nuclear layer. Scale bars = 1 μm (A and B), 500 nm (C and D), and 1 μm (E and F).
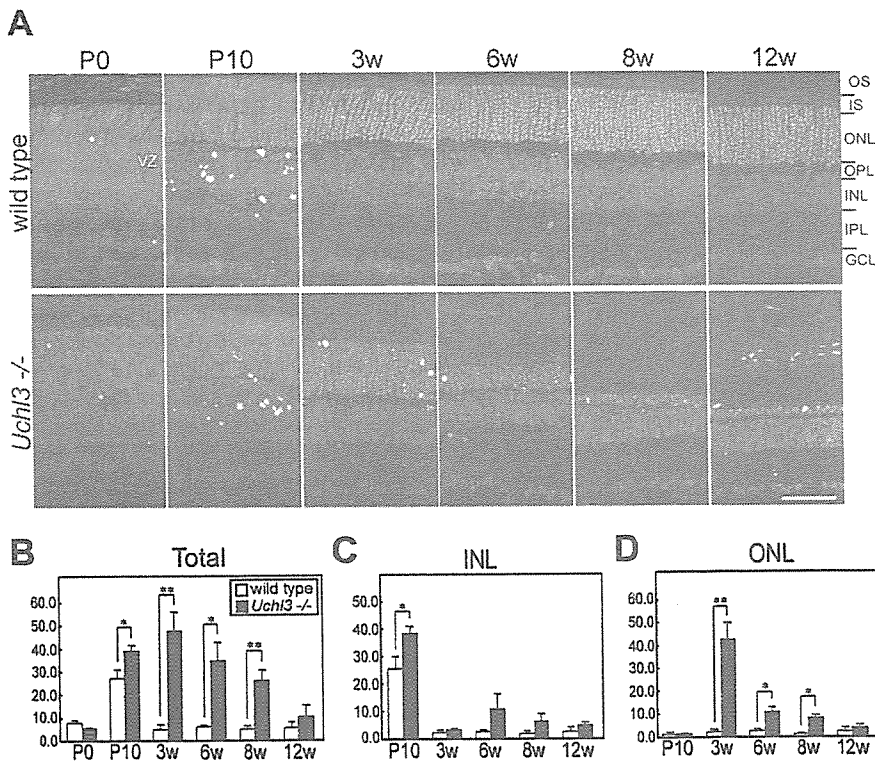
A

B Total   **C** INL   **D** ONL

cient mice may be due to caspase-independent apoptotic pathway (Figure 7). Ubiquitin and Nedd-8, which are considered to be associated with UCH-L3 *in vitro*,[14,15] were expressed in the inner retina of both genotypes in a similar pattern as UCH-L1 (data not shown).

Discussion

This study demonstrates the unique localization of UCH-L3 to the photoreceptor inner segment that is abundantly populated with mitochondria after 3w of age in wild-type mice. The following features were found with regard to retinal degeneration in *Uchl3*-deficient mice. The retina showed no obvious morphological abnormalities during early postnatal development; however, progressive retinal degeneration was observed after 3w of age. The inner segment was originally perturbated with ultrastructural changes of mitochondria and increased expressions of markers for oxidative stress. The caspase-independent pathway was implicated during photoreceptor cell apoptosis. Thus, UCH-L3 may have a role in preventing mitochondrial oxidative stress-related apoptosis in photoreceptor cells.

Differential Localization of UCH-L1 and UCH-L3 in Murine Retina

The cellular distribution of UCH-L3 has not been studied except in the testis and epididymis, where UCH-L1 and UCH-L3 have distinct expression patterns.[25] In the present study, we found that UCH-L3 was enriched in the photoreceptor inner segment after 3w of age, whereas

UCH-L1 was widely expressed in the inner retina. Photoreceptor cells are highly differentiated, and each segment has specific morphology and function; eg, inner segment contains abundant mitochondria,[27] and its oxygen consumption is considered to be high.[28] Meanwhile, expression of UCH-L1 at the inner retina was associated with that of ubiquitin and Nedd-8. Although *in vitro* studies indicate that UCH-L3 has de-neddylation activity,[14] UCH-L1 may be responsible for regulating expression level of ubiquitin and ubiquitin-like protein Nedd-8 in the retina. Because UCH-L1 expression in the retina was not altered in *Uchl3*-deficient mice, the function of UCH-L3 may not be compensated by UCH-L1. Our results indicate that UCH-L3 and UCH-L1 differ with regard to their localization and function in retina.

Mechanism of Photoreceptor Cell Death in the Uchl3-Deficient Mice

In our result, retinal apoptosis in *Uchl3*-deficient mice consisted of two different phases, during retinal development and after development. During the early postnatal development at P10, TUNEL-positive cells were observed in the inner nuclear layer of both genotypes, and the physiological apoptosis was slightly enhanced in the mutant retina. Because UCH-L3 was faintly expressed in the outer plexiform layer at P10 in wild-type mice, UCH-L3 may function during development. In the retinal development, the number of bipolar and Müller cell deaths reaches a peak at the postnatal days 8 to 11, which is associated with differentiation of the retina in
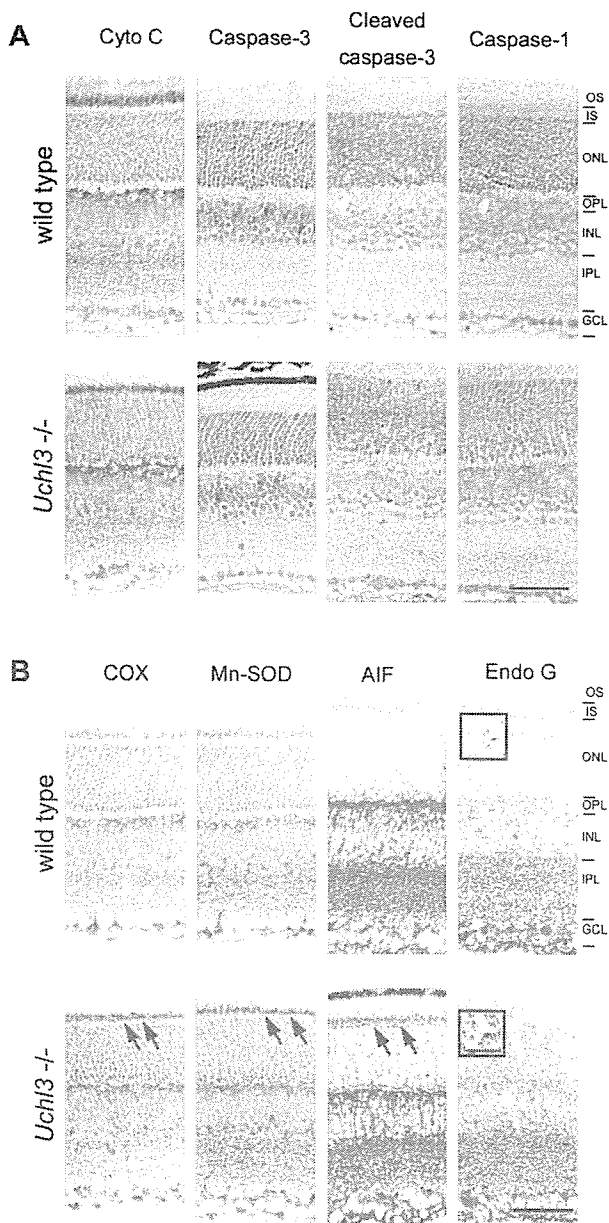
Figure 6. Immunohistochemical analysis of apoptosis- and oxidative stress-related molecules at 3w of age in wild-type and *Uchl3*-deficient mice. **A:** Expression of molecules relevant to the caspase-dependent pathway, including cytochrome *c* (Cyto C), caspase-3, cleaved caspase-3, and caspase-1, is unchanged between both genotypes. **B:** Increased immunoreactivities for oxidative stress markers, COX, Mn-SOD, and AIF, are observed in the inner segment of *Uchl3*-deficient mice (**arrows**). Translocation of Endo G to nuclei is found in the outer nuclear layer of *Uchl3*-deficient mice (**inset in B**). OS, outer segment; IS, inner segment; ONL, outer nuclear layer; OPL, outer plexiform layer; INL, inner nuclear layer; IPL, inner plexiform layer; GCL, ganglion cell layer. Scale bars = 50 μm (A and B); 10 μm (**inset in B**).

mice.[29] Therefore, loss of UCH-L3 may mildly promote the cell death of these cells.

After 3w of age, prominent and progressive photoreceptor cell apoptosis was disclosed in the outer nuclear layer of *Uchl3*-deficient mice. Under pathological conditions, several apoptotic pathways have been suggested in experimental retinal degeneration. Caspase-1 is predominantly associated with photoreceptor cell apoptosis in retinal degeneration of isch-

emia-reperfusion.[30] Light-induced retinal degeneration activates the parallel cascades, caspase-1[20] and caspase-independent apoptosis.[21] Oxidative stress leads to caspase-independent apoptosis in cultured cells.[31] Our results indicated that a caspase-independent pathway was activated during photoreceptor cell apoptosis in *Uchl3*-deficient mice, because immunohistochemical analysis revealed that activated caspase-3 and caspase-1 were not expressed in the degenerated retina. In addition, Endo G, a protein involved in the caspase-independent pathway, was expressed in the nuclei of the outer nuclear layer in *Uchl3*-deficient mice. Endo G is a mitochondria-specific nuclease that translocates to nuclei and serves as the DNase during a caspase-independent apoptosis.[32] Therefore, Endo G may be responsible for the DNA degradation that occurs during apoptosis in *Uchl3*-deficient mice. Expression of Endo G was slightly increased in the outer plexiform layer, inner nuclear layer, and inner plexiform layer of the *Uchl3*-deficient mice after 3w of age despite no significant UCH-L3 immunoreactivities in these layers. This result may reflect trans-synaptic secondary neuronal degeneration or glial changes of Müller cells.

AIF, another factor involved in caspase-independent apoptosis, was enriched in the inner segment; however, we did not observe translocation to nuclei for this protein. AIF is a mitochondrial flavoprotein that is a free radical scavenger of healthy cells.[33] During apoptotic induction, AIF translocates from mitochondria to nuclei.[33,34] It functions as a caspase-independent and PARP-1-dependent death effector that induces chromatin condensation and large-scale DNA fragmentation.[35] In our study, expression of AIF at the inner segment was associated with increased immunoreactivities of the oxidative stress markers, COX and Mn-SOD. Although it is unknown why AIF did not translocate to nuclei in the degenerated retina, increased immunoreactivity for AIF in the inner segment may indicate a reaction to oxidative stress. Because mouse eyes open 12 to 13 days after birth, light-induced oxidative stress may affect photoreceptor cell apoptosis in *Uchl3*-deficient mice after development. On the other hand, the retinal oxygen consumption increases under dark-adapted condition in the cat retina.[28,36] It may be interesting to study whether constant light or constant dark has any effect on the development of retinal degeneration in the *Uchl3*-deficient mice.

Uchl3-Deficient Mice as a Model of Retinal Degeneration with Mitochondrial Impairment

Apoptosis during retinal degeneration is observed in inherited diseases such as retinitis pigmentosa as well as in retinal diseases induced by a variety of stimuli, including hypoxia and oxidative stresses.[37,38] Several genetically engineered animal models of retinitis pigmentosa have been extensively investigated, including the RCS rat and *rd* mice. Retinal degeneration in the RCS rat was originally identified as an impairment of phagocytosis by pigmented epithelium due to mutation of receptor ty-

Table 1. Chronological Changes in Expression of Markers for Oxidative Stress and Caspase-Independent Apoptosis

	COX						Mn-SOD						AIF						Endo G					
	P0	P10	3w	6w	8w	12w	P0	P10	3w	6w	8w	12w	P0	P10	3w	6w	8w	12w	P0	P10	3w	6w	8w	12w
VZ*	−						−						−						−					
PR		−						−						−						−				
OS			−	−	nd	nd			−	−	nd	nd			−	−	nd	nd			−	−	nd	nd
IS			+	+	−	nd			+	+	+	nd			++	+	−	nd			−	−	−	nd
ONL	−	−	−	−	−		−	−	−	−	−		−	−	−	−	−		−		++§	+§	−	−
OPL	−	−	−	−	−		−	−	−	−	−		−	−	−	−	−		−		±	±	±	±
INL	−	−	−	−	−		−	−	−	−	−		−	−	−	−	−		−		±§	±§	−	−
IPL	−	−	−	−	−	−	−	−	−	−	−	−	−	−	−	−	−	−	−		−	−	±	±
GCL	−	−	−	−	−	−	−	−	−	−	−	−	−	−	−	−	−	−	−		−	−	−	−

*VZ, ventricular zone; PR, photoreceptor; OS, outer segment; IS, inner segment; ONL, outer nuclear layer; OPL, outer plexiform layer; INL, inner nuclear layer; IPL, inner plexiform layer; GCL, ganglion cell layer.
−, no change; ±, slight increase; +, mild increase; and ++, marked increase of immunoreactivity compared to that of wild type.
nd, not determined due to atrophic change.
§Nuclear staining.

rosine kinase (Mertk) with subsequent photoreceptor cell death occurring in a caspase-1- and -2-dependent manner.[39–42] rd mice have a recessive mutation in the rod cGMP phosphodiesterase β-subunit, and photoreceptor apoptosis occurs via a caspase-dependent mechanism.[43,44] Thus, these animal models of retinitis pigmentosa differ from Uchl3-deficient mice with regard to the mechanism of retinal degeneration.

The relationship between retinal degeneration and mitochondrial dysfunction has not been well studied except in Harlequin mice, which contain a mutation of AIF and exhibit progressive retinal degeneration.[45] We consider that the degeneration induced in the Uchl3-deficient mice is associated with mitochondrial dysfunction, because mitochondria in the inner segment of mutant retina exhibited morphological changes such as decreased cristae area. Uchl3-deficient mice reveal not only retinal degeneration but also muscle degeneration and mild growth

retardation,[17] and thus the lack of UCH-L3 may affect general organs containing abundant mitochondria. Subtypes of mitochondrial diseases, such as chronic progressive external ophthalmoplegia and Kearns-Sayre syndrome, are caused by various mitochondrial DNA deletions and observed progressive ophthalmoplegia as well as retinitis pigmentosa.[46,47] Because UCH-L3 is predicted to be involved in the maintenance of mitochondrial function, Uchl3-deficient mice may be a model of disease that arises from mitochondrial impairment. Further studies are necessary to clarify the molecular mechanisms underlying retinal degeneration, as well as other organs in these animals.
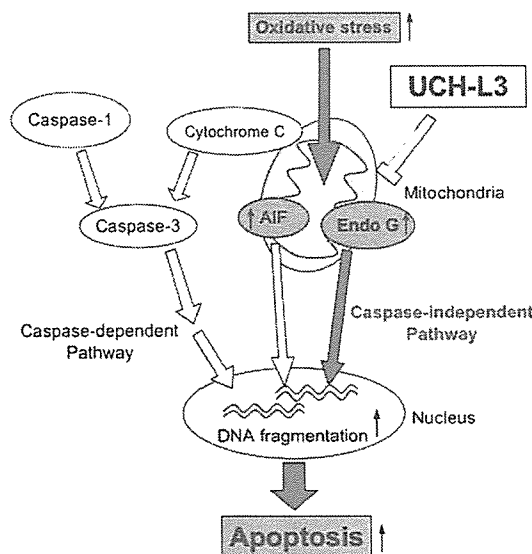
Acknowledgments

Figure 7. Function of UCH-L3 in apoptosis during retinal degeneration. Mitochondrial apoptosis is classified into caspase-dependent and caspase-independent pathways. Loss of UCH-L3 leads to oxidative stress-induced mitochondrial damage that causes translocation of Endo G from mitochondria to nuclei, resulting in caspase-independent apoptosis. **Red arrows** are considered to be activated in Uchl3-deficient mice.

References

1. Amerik AY, Hochstrasser M: Mechanism and function of deubiquitinating enzymes. Biochim Biophys Acta 2004, 1695:189–207
2. Weissman AM: Themes and variations on ubiquitylation. Nat Rev Mol Cell Biol 2001, 2:169–178
3. Pickart CM, Eddins MJ: Ubiquitin: structures, functions, mechanisms. Biochim Biophys Acta 2004, 1695:55–72
4. Aguilar RC, Wendland B: Ubiquitin: not just for proteasomes anymore. Curr Opin Cell Biol 2003, 15:184–190
5. Wilkinson KD: Regulation of ubiquitin-dependent processes by deubiquitinating enzymes. FASEB J 1997, 11:1245–1256
6. Doran JF, Jackson P, Kynoch PA, Thompson RJ: Isolation of PGP 9.5, a new human neurone-specific protein detected by high-resolution two-dimensional electrophoresis. J Neurochem 1983, 40:1542–1547
7. Wilkinson KD, Lee KM, Deshpande S, Duerksen-Hughes P, Boss JM, Pohl J: The neuron-specific protein PGP 9.5 is a ubiquitin carboxyl-terminal hydrolase. Science 1989, 246:670–673
8. Osawa Y, Wang YL, Osaka H, Aoki S, Wada K: Cloning, expression, and mapping of a mouse gene, Uchl4, highly homologous to human and mouse Uchl3. Biochem Biophys Res Commun 2001, 283:627–633

9. Liu Y, Fallon L, Lashuel HA, Liu Z, Lansbury PT Jr,: The UCH-L1 gene encodes two opposing enzymatic activities that affect alpha-synuclein degradation and Parkinson's disease susceptibility. Cell 2002, 111:209–218

10. Leroy E, Boyer R, Auburger G, Leube B, Ulm G, Mezey E, Harta G, Brownstein MJ, Jonnalagada S, Chernova T, Dehejia A, Lavedan C, Gasser T, Steinbach PJ, Wilkinson KD, Polymeropoulos MH: The ubiquitin pathway in Parkinson's disease. Nature 1998, 395:451–452

11. Saigoh K, Wang YL, Suh JG, Yamanishi T, Sakai Y, Kiyosawa H, Harada T, Ichihara N, Wakana S, Kikuchi T, Wada K: Intragenic deletion in the gene encoding ubiquitin carboxy-terminal hydrolase in *gad* mice. Nat Genet 1999, 23:47–51

12. Wilkinson KD, Deshpande S, Larsen CN: Comparisons of neuronal (PGP 9.5) and non-neuronal ubiquitin C-terminal hydrolases. Biochem Soc Trans 1992, 20:631–637

13. Kurihara LJ, Semenova E, Levorse JM, Tilghman SM: Expression and functional analysis of *Uch-L3* during mouse development. Mol Cell Biol 2000, 20:2498–2504

14. Wada H, Kito K, Caskey LS, Yeh ET, Kamitani T: Cleavage of the C-terminus of NEDD8 by UCH-L3. Biochem Biophys Res Commun 1998, 251:688–692

15. Gan-Erdene T, Nagamalleswari K, Yin L, Wu K, Pan ZQ, Wilkinson KD: Identification and characterization of DEN1, a deneddylase of the ULP family. J Biol Chem 2003, 278:28892–28900

16. Kwon J, Wang YL, Setsuie R, Sekiguchi S, Sato Y, Sakurai M, Noda M, Aoki S, Yoshikawa Y, Wada K: Two closely related ubiquitin C-terminal hydrolase isozymes function as reciprocal modulators of germ cell apoptosis in cryptorchid testis. Am J Pathol 2004, 165:1367–1374

17. Semenova E, Wang X, Jablonski MM, Levorse J, Tilghman SM: An engineered 800 kilobase deletion of *Uchl3* and *Lmo7* on mouse chromosome 14 causes defects in viability, postnatal growth and degeneration of muscle and retina. Hum Mol Genet 2003, 12:1301–1312

18. Chang GQ, Hao Y, Wong F: Apoptosis: final common pathway of photoreceptor death in rd, rds, and rhodopsin mutant mice. Neuron 1993, 11:595–605

19. Cook B, Lewis GP, Fisher SK, Adler R: Apoptotic photoreceptor degeneration in experimental retinal detachment. Invest Ophthalmol Vis Sci 1995, 36:990–996

20. Grimm C, Wenzel A, Hafezi F, Remè CE: Gene expression in the mouse retina: the effect of damaging light. Mol Vis 2000, 6:252–260

21. Donovan M, Cotter TG: Caspase-independent photoreceptor apoptosis in vivo and differential expression of apoptotic protease activating factor-1 and caspase-3 during retinal development. Cell Death Differ 2002, 9:1220–1231

22. Osborne NN, Melena J, Chidlow G, Wood JP: A hypothesis to explain ganglion cell death caused by vascular insults at the optic nerve head: possible implication for the treatment of glaucoma. Br J Ophthalmol 2001, 85:1252–1259

23. Adler R, Curcio C, Hicks D, Price D, Wong F: Cell death in age-related macular degeneration. Mol Vis 1999, 5:31

24. Harada T, Harada C, Wang YL, Osaka H, Amanai K, Tanaka K, Takizawa S, Setsuie R, Sakurai M, Sato Y, Noda M, Wada K: Role of ubiquitin carboxy terminal hydrolase-L1 in neural cell apoptosis induced by ischemic retinal injury in vivo. Am J Pathol 2004, 164:59–64

25. Kwon J, Wang YL, Setsuie R, Sekiguchi S, Sakurai M, Sato Y, Lee WW, Ishii Y, Kyuwa S, Noda M, Wada K, Yoshikawa Y: Developmental regulation of ubiquitin C-terminal hydrolase isozyme expression during spermatogenesis in mice. Biol Reprod 2004, 71:515–521

26. Osaka H, Wang YL, Takada K, Takizawa S, Setsuie R, Li H, Sato Y, Nishikawa K, Sun YJ, Sakurai M, Harada T, Hara Y, Kimura I, Chiba S, Namikawa K, Kiyama H, Noda M, Aoki S, Wada K: Ubiquitin carboxy-terminal hydrolase L1 binds to and stabilizes monoubiquitin in neuron. Hum Mol Genet 2003, 12:1945–1958

27. De Robertis E: Electron microscope observations on the submicro-

28. Linsenmeier RA, Braun RD: Oxygen distribution and consumption in the cat retina during normoxia and hypoxemia. J Gen Physiol 1992, 99:177–197

29. Young RW: Cell death during differentiation of the retina in the mouse. J Comp Neurol 1984, 229:362–373

30. Katai N, Yoshimura N: Apoptotic retinal neuronal death by ischemia-reperfusion is executed by two distinct caspase family proteases. Invest Ophthalmol Vis Sci 1999, 40:2697–2705

31. Carmody RJ, Cotter TG: Oxidative stress induces caspase-independent retinal apoptosis in vitro. Cell Death Differ 2000, 7:282–291

32. Li LY, Luo X, Wang X: Endonuclease G is an apoptotic DNase when released from mitochondria. Nature 2001, 412:95–99

33. Susin SA, Lorenzo HK, Zamzami N, Marzo I, Snow BE, Brothers GM, Mangion J, Jacotot E, Costantini P, Loeffler M, Larochette N, Goodlett DR, Aebersold R, Siderovski DP, Penninger JM, Kroemer G: Molecular characterization of mitochondrial apoptosis-inducing factor. Nature 1999, 397:441–446

34. Lorenzo HK, Susin SA, Penninger J, Kroemer G: Apoptosis inducing factor (AIF): a phylogenetically old, caspase-independent effector of cell death. Cell Death Differ 1999, 6:516–524

35. Yu SW, Wang H, Poitras MF, Coombs C, Bowers WJ, Federoff HJ, Poirier GG, Dawson TM, Dawson VL: Mediation of poly(ADP-ribose) polymerase-1-dependent cell death by apoptosis-inducing factor. Science 2002, 297:259–263

36. Linsenmeier RA: Effects of light and darkness on oxygen distribution and consumption in the cat retina. J Gen Physiol 1986, 88:521–542

37. Pacione LR, Szego MJ, Ikeda S, Nishina PM, McInnes RR: Progress toward understanding the genetic and biochemical mechanisms of inherited photoreceptor degenerations. Annu Rev Neurosci 2003, 26:657–700

38. Phelan JK, Bok D: A brief review of retinitis pigmentosa and the identified retinitis pigmentosa genes. Mol Vis 2000, 6:116–124

39. D'Cruz PM, Yasumura D, Weir J, Matthes MT, Abderrahim H, LaVail MM, Vollrath D: Mutation of the receptor tyrosine kinase gene Mertk in the retinal dystrophic RCS rat. Hum Mol Genet 2000, 9:645–651

40. Feng W, Yasumura D, Matthes MT, LaVail MM, Vollrath D: Mertk triggers uptake of photoreceptor outer segments during phagocytosis by cultured retinal pigment epithelial cells. J Biol Chem 2002, 277:17016–17022

41. Katai N, Kikuchi T, Shibuki H, Kuroiwa S, Arai J, Kurokawa T, Yoshimura N: Caspase-like proteases activated in apoptotic photoreceptors of Royal College of Surgeons rats. Invest Ophthalmol Vis Sci 1999, 40:1802–1807

42. Vollrath D, Feng W, Duncan JL, Yasumura D, D'Cruz PM, Chappelow A, Matthes MT, Kay MA, LaVail MM: Correction of the retinal dystrophy phenotype of the RCS rat by viral gene transfer of Mertk. Proc Natl Acad Sci USA 2001, 98:12584–12589

43. Jomary C, Neal MJ, Jones SE: Characterization of cell death pathways in murine retinal neurodegeneration implicates cytochrome c release, caspase activation, and bid cleavage. Mol Cell Neurosci 2001, 18:335–346

44. Lem J, Flannery JG, Li T, Applebury ML, Farber DB, Simon MI: Retinal degeneration is rescued in transgenic rd mice by expression of the cGMP phosphodiesterase β subunit. Proc Natl Acad Sci USA 1992, 89:4422–4426

45. Klein JA, Longo-Guess CM, Rossmann MP, Seburn KL, Hurd RE, Frankel WN, Bronson RT, Ackerman SL: The harlequin mouse mutation downregulates apoptosis-inducing factor. Nature 2002, 419:367–374

46. Land JM, Morgan-Hughes JA, Hargreaves I, Heales SJ: Mitochondrial disease: a historical, biochemical, and London perspective. Neurochem Res 2004, 29:483–491

47. Schmiedel J, Jackson S, Schäfer J, Reichmann H: Mitochondrial cytopathies. J Neurol 2003, 250:267–277

scopic organization of the retinal rods. J Biophys Biochem Cytol 1956, 2:319–330